Electronic Supplementary Material (ESI) for Organic & Biomolecular Chemistry.

Supporting Information

Helical peptaibol mimics are better ionophores when racemic than when enantiopure

Sarah J. Pike,[‡a,b] Jennifer E. Jones,[‡a,b] James Raftery,[a] Jonathan Clayden,[a]* and Simon J. Webb[a,b]*

[a] School of Chemistry, University of Manchester, Oxford Road, Manchester, M13 9PL, UK.

[b] Manchester Institute of Biotechnology, University of Manchester, 131 Princess St., Manchester, M1 7DN, UK.

Email: S.Webb@manchester.ac.uk, clayden@man.ac.uk

General Experimental Section

Nuclear Magnetic Resonance (NMR) spectra were recorded on a Bruker Ultraseld 300, 400 or 500 MHz spectrometer. ^{1}H and ^{13}C spectra were referenced relative to the solvent residual peaks and chemical shifts (δ) reported in ppm downfield of tetramethylsilane ($CDCl_3$ δ H: 7.26 ppm, δ C: 77.0 ppm). Coupling constants (J) are reported in Hertz and rounded to 0.1 Hz. Splitting patterns are abbreviated as follows: singlet (s), doublet (d), multiplet (m), septet (spt), broad (br) or some combination of these.

Low and high resolution mass spectra were recorded by staff at the University of Manchester. Electrospray (ES) spectra were recorded on a Waters Platform II and high resolution mass spectra (HRMS) were recorded on a Thermo Finnigan MAT95XP and are accurate to ± 0.001 Da. Infrared spectra were recorded on a Thermo Scientific Nicolet iS5 FTIR Spectrometer. Melting points were determined on a GallenKamp apparatus and are uncorrected. Thin layer chromatography (TLC) was performed using commercially available pre-coated plates (Macherey-Nagel alugram. Sil G/UV254) and visualized with UV light at 254 nm; phosphomolybdic acid dip was used to reveal the products. Flash column chromatography was carried out using Fluorochem Davisil 40-63u 60Å.

All reactions were conducted under a nitrogen atmosphere in oven-dried glassware unless stated otherwise. Dichloromethane was obtained by distillation over calcium hydride under a nitrogen atmosphere. All other solvents and commercially available reagents were used as received.

Procedures for the synthesis of H_2N-Aib_4O^t-Bu,[1] Cbz-L-Phe-Aib_4O^t-Bu,[2] Cbz-D-Phe-Aib_4O^t-Bu,[2] Cbz-L-(αMeVal)-Aib_4O^t-Bu[2] and Cbz-L-(αMe)ValF[3] have been reported previously. The following abbreviations have been used; Aib = aminoisobutyric acid,

Cbz = carboxybenzyl, DIPEA = *N*,*N*,-diisopropylethylamine, EtOAc = ethyl acetate, Et_2O = di-ethyl ether, (αMe)Val = α-methylvaline, Phe = Phenylalanine, ^{t}Bu = tert-butyl

Synthetic Details

Cbz-(*rac*)-PheAib$_4$O^{t}Bu

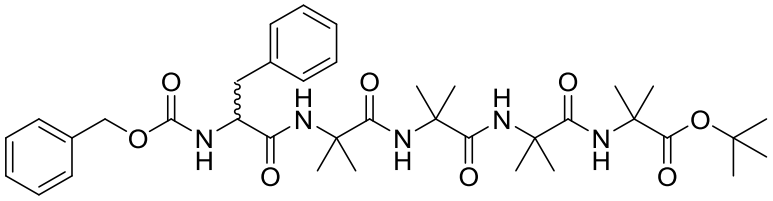

A solution of Cbz-L-PheAib$_4$O^{t}Bu (0.050 g, 0.072 mmol) in CH_2Cl_2 (3 mL) was added Cbz-D-PheAib$_4$O^{t}Bu (0.050 g, 0.072 mmol) and the reaction mixture was left stirring at ambient temperature for 10 mins. After this time, the excess solvent was removed under reduced pressure to give a white solid. **m.p.** (powder) 248-250 ºC; ^{1}H NMR (500 MHz, $CDCl_3$); δ = 7.38 – 7.27 (m, 9H, Ar*H* + N*H*), 7.18 (d, 2H, J = 6.8 Hz, Ar*H*), 7.10 (s, br, 1H, N*H*), 6.92 (s, br, 1H, N*H*), 6.13 (s, br, 1H, N*H*), 5.37 (d, 1H, J = 12.0 Hz, N*H*), 5.10 (d, A of AB, 1H, J = 12.2 Hz, C*H* of CH_2), 5.07 (d, B of AB, 1H, J = 12.2 Hz, C*H* of CH_2), 4.11 – 4.09 (m, 1H, C*H*), 3.13 (dd, 1H, J = 14.0 Hz, ^{4}J = 6.4 Hz, C*H* of CH_2), 2.99 (dd, 1H, J = 14.0 Hz, ^{4}J = 8.2 Hz, C*H* of CH_2), 1.51 (6H, s, 2 × CH_3, Aib), 1.47 (6H, s, 2 × CH_3, Aib), 1.43 (9H, s, 3 × CH_3, O^{t}Bu), 1.41 (3H, s, CH_3, Aib), 1.40 (3H, s, CH_3, Aib), 1.34 (3H, s, CH_3, Aib), 1.27 (3H, s, CH_3, Aib), ^{13}C NMR (125 MHz, $CDCl_3$); 174.1 (CO), 173.7 (CO), 173.2 (CO), 173.0 (CO), 171.0 (CO), 170.8 (CO), 135.8 (Ar), 135.7 (Ar), 129.2 (Ar), 129.0 (Ar), 128.7 (2C, Ar), 128.6 (Ar), 128.2 (2C, Ar), 127.5 (Ar), 79.9 (αC, O^{t}Bu), 67.6 (CH_2), 57.5 (*C*H), 57.0 (αC, Aib), 56.9 (αC, Aib), 56.7 (αC, Aib), 56.1 (αC, Aib), 36.7 (CH_2), 27.9

(CH_3,O^{t}Bu), 25.6 (CH_3, Aib), 25.4 (CH_3, Aib), 25.34 (CH_3, Aib), 25.30 (CH_3, Aib), 25.0 (CH_3, Aib), 24.8 (CH_3, Aib), 24.7 (CH_3, Aib), 24.6 (CH_3, Aib); **IR** 3324, 2983, 2933, 1707, 1665, 1526, 1467, 1455, 1384, 1364, 1258, 1148, 1028; **MS** (ES^+, MeOH): *m/z* = 695 ($[M+H]^+$, 12%), 719 ($[M+Na]^+$, 8%).

Cbz-D-(αMe)ValAib$_4$O^{t}Bu

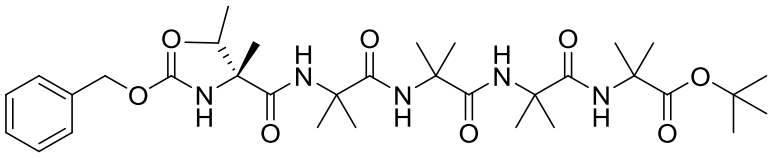

A stirred solution of H_2NAib$_4$O^{t}Bu (0.30 g, 0.72 mmol) and DIPEA (0.25 mL, 1.45 mmol) in CH_2Cl_2 (15 mL) was cooled to 0 °C and a solution of Cbz-D-(αMe)Val-F (0.39 g, 1.45 mmol) in CH_2Cl_2 (4 mL) was added and the reaction stirred at room temperature for 6 days. The solvent was removed under reduced pressure and the resulting residue re-dissolved in EtOAc (50 mL) and washed with 5% $KHSO_4$ solution (2 × 20 mL), sat. $NaHCO_3$ solution (2 × 20 mL) and brine (20 mL). The organic layer was dried ($MgSO_4$) and concentrated under reduced pressure. Trituration of the resulting oily solid with Et_2O gave the desired compound as a white solid. (0.34 g, 72%) **m.p.** (powder) 215-216 ºC; ^{1}H NMR (500 MHz, $CDCl_3$); δ = 7.43 (s, br, 1H, N*H*), 7.37 – 7.35 (m, 5H, Ar*H*), 7.32 (s, br, 1H, N*H*), 7.27 (s, br, 1H, N*H*), 6.25 (s, br, 1H, N*H*), 5.33 (s, br, 1H, N*H*), 5.18 (d, A of AB, 1H, J = 12.2 Hz, C*H* of CH_2), 5.02 (d, B of AB, 1H, J = 12.2 Hz, C*H* of CH_2), 1.92 (spt, 1H, C*H*(CH_3)$_2$), 1.54 (s, 3H, CH_3), 1.49 (s, 3H, CH_3), 1.47 (s, 3H, CH_3), 1.46 (s, 3H, CH_3), 1.45 (s, 6H, 2 × CH_3), 1.41 (s, 9H, 3 × CH_3), 1.41 (s, 6H, 2 × CH_3), 1.20 (s, 3H, CH_3), 0.97 (d, J = 6.8 Hz, 3H, CH(CH_3)), 0.93 (d, J = 6.8 Hz, 3H, CH(CH_3)); ^{13}C NMR (75 MHz, $CDCl_3$); 174.1 (CO), 173.9 (CO), 173.65 (CO), 173.59 (CO), 172.35 (CO),

156.0 (CO), 135.9 (Ar), 128.71 (Ar), 128.65 (Ar), 128.3 (Ar), 79.7 (αC, O^{t}Bu), 67.4 (*C*H$_2$), 63.0 (αC), 56.9 (αC, Aib), 56.7 (αC, Aib), 56.6 (αC, Aib), 56.0 (αC, Aib), 35.5 (*C*H(CH$_3$)$_2$), 27.8 (CH$_3$), 25.5 (CH$_3$), 24.0 (CH$_3$), 23.7 (CH$_3$), 23.5 (CH$_3$), 17.6 (*C*H$_3$), 17.2 (CH(*C*H$_3$)$_2$), 17.1 (CH(*C*H$_3$)$_2$); **IR** 3424, 3316, 3255, 2979, 2939, 1729, 1698, 1680, 1668, 1642, 1531, 1499, 1456, 1383, 1362, 1310, 1266, 1225, 1214, 1147, 1071, 1038; **MS** (ES$^+$, MeOH): *m/z* = 663 ([M+H]$^+$, 15%), 685 ([M+Na]$^+$, 100%), 701 ([M+K]$^+$, 37%).

Cbz-(*rac*)-(αMe)ValAib$_4$O^{t}Bu

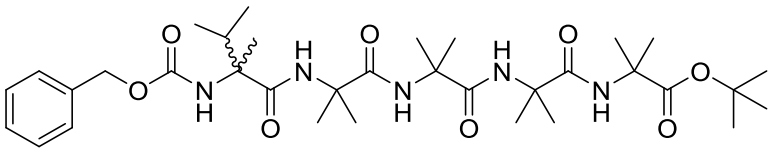

A solution of Cbz-L-(αMe)ValAib$_4$O^{t}Bu (0.030 g, 0.045 mmol) in CH_2Cl_2 (2 mL) was added Cbz-D-(αMe)ValAib$_4$O^{t}Bu (0.030 g, 0.045 mmol) and the reaction mixture was left stirring at ambient temperature for 10 mins. After this time, the excess solvent was removed under reduced pressure and to give a white solid. **m.p.** 239-241 ^{o}C; ^{1}H NMR (400 MHz, $CDCl_3$); δ = 7.42 (s, br, 1H, N*H*), 7.38 – 7.31 (m, 5H, Ar*H*), 7.31 (s, br, 1H, N*H*), 7.25 (s, br, 1H, N*H*), 6.22 (s, br, 1H, N*H*), 5.19 (d, A of AB, 1H, J = 12.2 Hz, C*H* of C*H*$_2$), 5.15 (s, br, 1H, N*H*), 5.03 (d, B of AB, 1H, J = 12.2 Hz, C*H* of C*H*$_2$), 1.91 (spt, 1H, C*H*(CH$_3$)$_2$), 1.48 (s, 3H, C*H*$_3$), 1.47 (s, 3H, C*H*$_3$), 1.45 (s, 6H, 2 × C*H*$_3$), 1.42 (s, 6H, 2 × C*H*$_3$), 1.41 (s, 15H, 5 × C*H*$_3$), 1.21 (s, 3H, C*H*$_3$), 0.97 (d, J = 6.8 Hz, 3H, CH(C*H*$_3$)), 0.94 (d, J = 6.9 Hz, 3H, CH(C*H*$_3$)); ^{13}C NMR (75 MHz, $CDCl_3$); 174.1 (CO), 173.8 (CO), 173.54 (CO), 173.51 (CO), 172.2 (CO), 155.9 (CO), 135.8 (Ar), 128.76 (Ar), 128.74 (Ar), 128.3 (Ar), 79.7 (αC, O^{t}Bu), 67.5 (*C*H$_2$), 63.0

(αC, Aib), 56.9 (αC, Aib), 56.70 (αC, Aib), 56.66 (αC, Aib), 56.0 (αC, Aib), 35.6 (*C*H(CH_3)$_2$), 27.9 (CH_3), 27.2 (CH_3), 26.89 (CH_3), 26.83 (CH_3), 25.5 (CH_3), 24.1 (CH_3), 23.7 (CH_3), 23.5 (CH_3), 23.4 (CH_3), 17.6 (*C*H_3), 17.2 (CH(*C*H_3)$_2$), 17.1 (CH(*C*H_3)$_2$); **IR** 3421, 3341, 3307, 3232, 2980, 2940, 2237, 1729, 1697, 1683, 1667, 1638, 1537, 1501, 1456, 1384, 1363, 1308, 1269, 1224, 1213, 1147, 1071, 1038; **MS** (ES^+, MeOH): *m/z* = 663 ($[M+H]^+$, 18%), 685 ($[M+Na]^+$, 42%), 701 ($[M+K]^+$, 14%).

DMSO-d_6 titrations and dilution studies.

In the following DMSO-d_6 titrations and dilution studies the protons are labelled alphabetically from low to high field. The two N-terminal NH protons are revealed by DMSO-d_6 titrations. Of these two, the NH of the Phe residue in **1** can be identified due to coupling to the adjacent α-CH. However unabiguous assignment is not possible with compound **2** as the MeVal has no α-CH. The other NH resonances remain unassigned.

DMSO-d_6 titrations

The 3_{10} helical conformations were confirmed in solution by titrating DMSO-d_6 into **(*S* or *rac*)-1** and **(*S* or *rac*)-2**.[4] See S. J. Pike, V. Diemer, J. Raftery, S. J. Webb and J. Clayden, Chem. Eur. J., 2014, 20, 15981–15990 and T. P. Pitner and D. W. Urry, J. Am. Chem. Soc., 1972, 94, 1399-1400.

DMSO-d_6 Titration for Cbz-L-PheAib$_4$O^{t}Bu

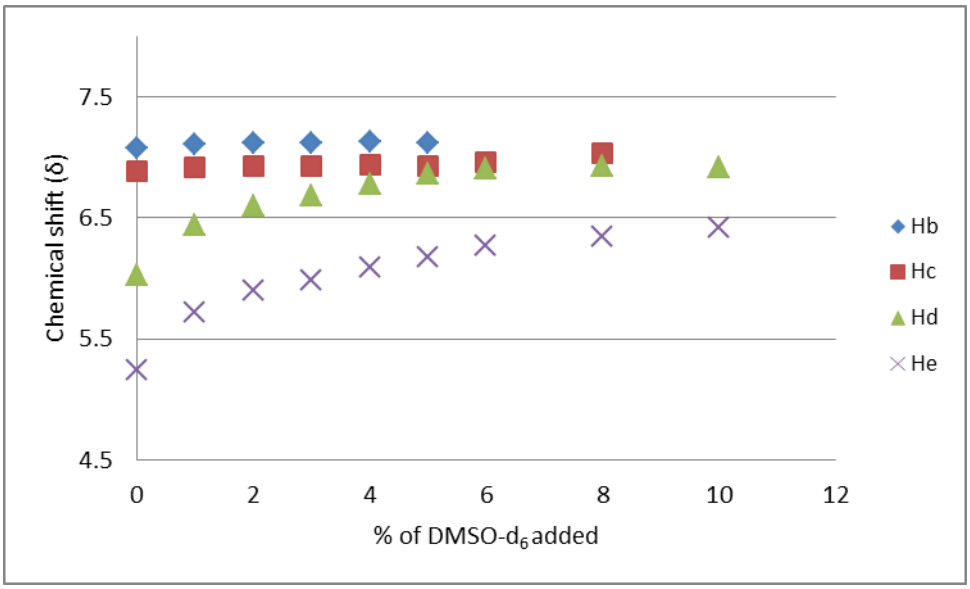

Graph S1: A graph to show the plot of % of DMSO *vs* chemical shift for the NH protons of a 0.005M solution of Cbz-L-PheAib$_4$O^{t}Bu.

DMSO-d_6 Titration for Cbz-(rac)-PheAib$_4$O^{t}Bu

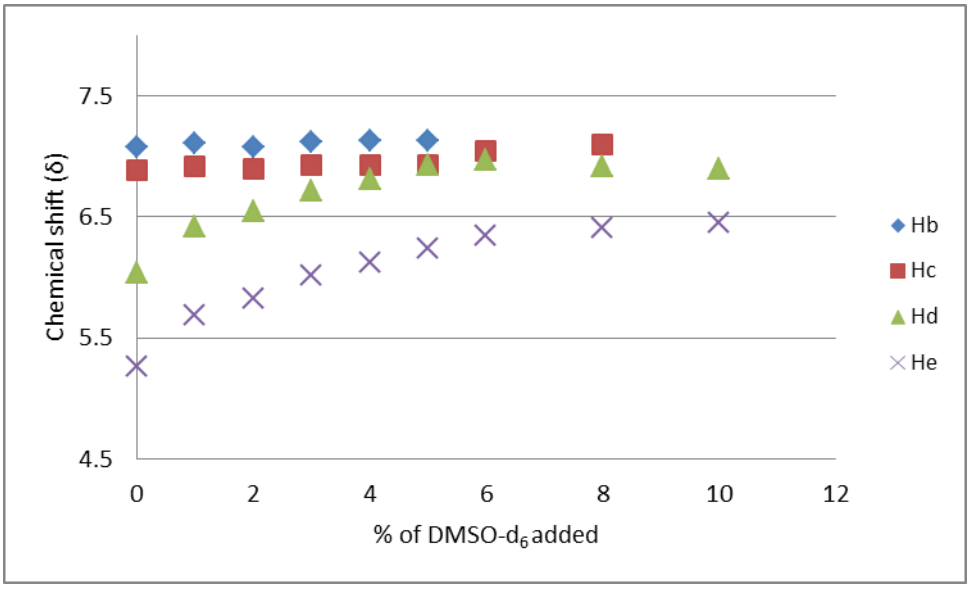

Graph S2: A graph to show the plot of % of DMSO *vs* chemical shift for the NH protons of a 0.005M solution of Cbz-(*rac*)-PheAib$_4$O^{t}Bu.

DMSO-d_6 Titration for Cbz-L-(αMe)ValAib$_4$O^{t}Bu

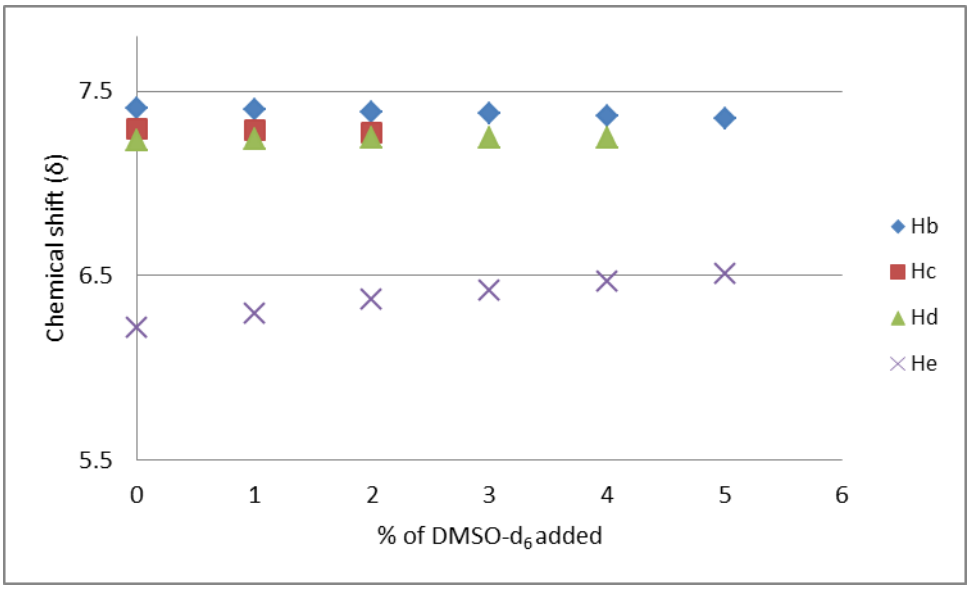

Graph S3: A graph to show the plot of % of DMSO *vs* chemical shift for the NH protons of a 0.005M solution of Cbz-L-(αMe)ValAib$_4$O^{t}Bu.

DMSO-d_6 Titration for Cbz-(rac)-(αMe)ValAib$_4$O^{t}Bu

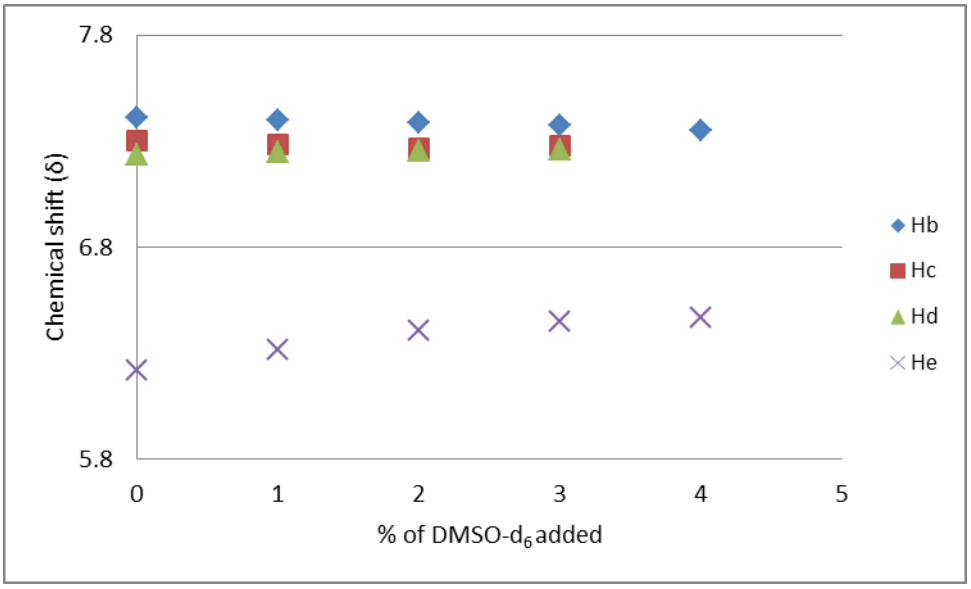

Graph S4: A graph to show the plot of % of DMSO *vs* chemical shift for the NH protons of a 0.005M solution of Cbz-(*rac*)-(αMe)ValAib$_4$O^{t}Bu.

NH Plots

Concentration Study for Cbz-L-PheAib$_4$O^{t}Bu

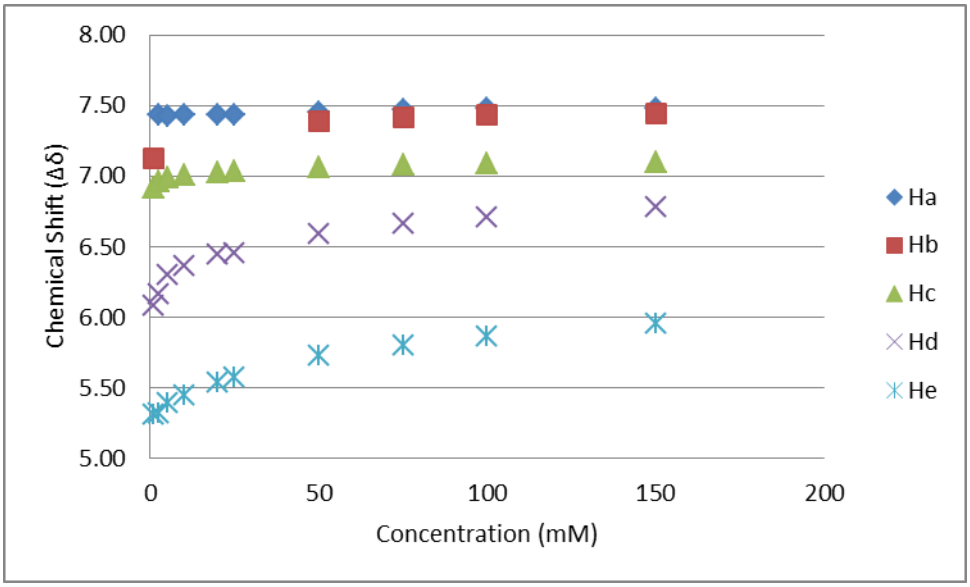

Graph S5: A graph to show the plot of concentration (M) *vs* chemical shift for the NH protons of Cbz-L-PheAib$_4$O^{t}Bu.

Concentration Study for Cbz-(rac)-PheAib$_4$O^{t}Bu

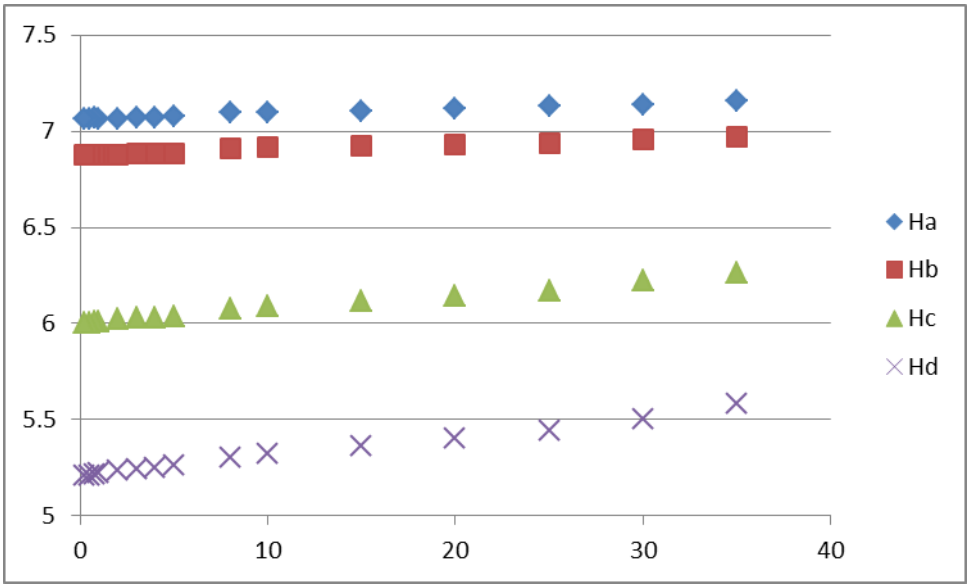

Graph S6: A graph to show the plot of concentration (M) *vs* chemical shift for the NH protons of Cbz-(*rac*)-PheAib$_4$O^{t}Bu.

Concentration Study for Cbz-L-(αMe)ValAib$_4$O^{t}Bu

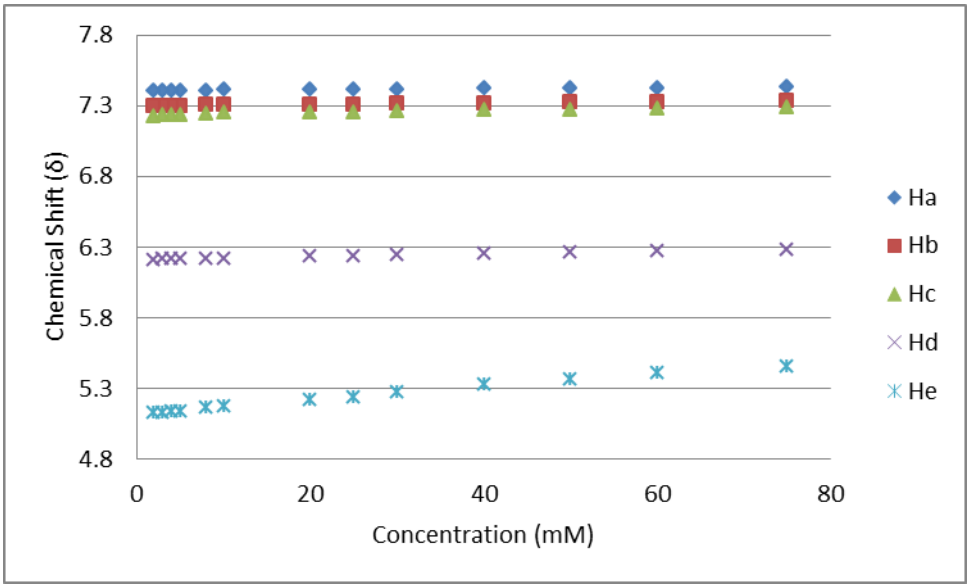

Graph S7: A graph to show the plot of concentration (M) *vs* chemical shift for the NH protons of Cbz-L-MeValAib$_4$O^{t}Bu.

Concentration Study for Cbz-(rac)-(αMe)ValAib$_4$O^{t}Bu

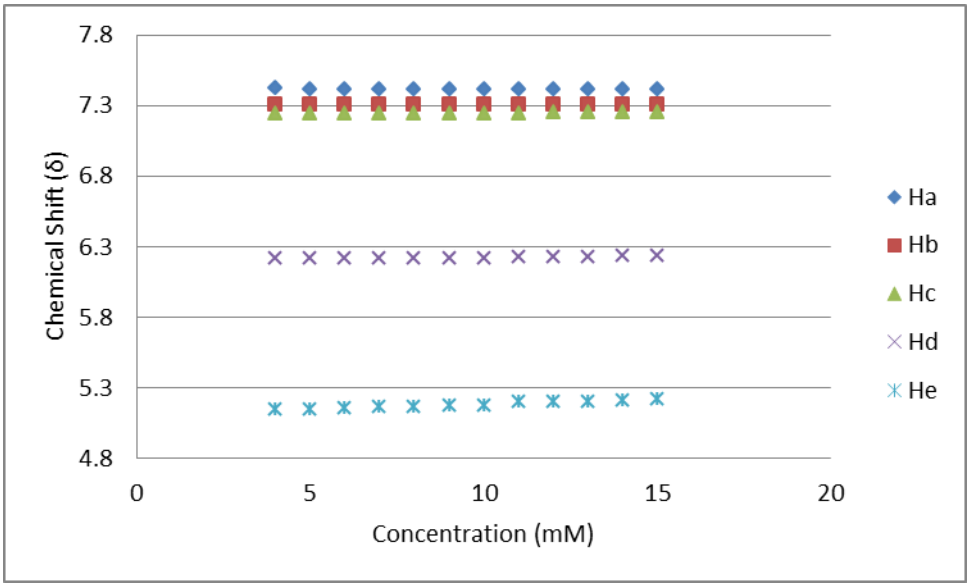

Graph S8: A graph to show the plot of concentration (M) *vs* chemical shift for the NH protons of Cbz-(*rac*)-(αMe)ValAib$_4$O^{t}Bu.

Stack Plots

Stack Plot for Cbz-L-PheAib$_4$O^{t}Bu

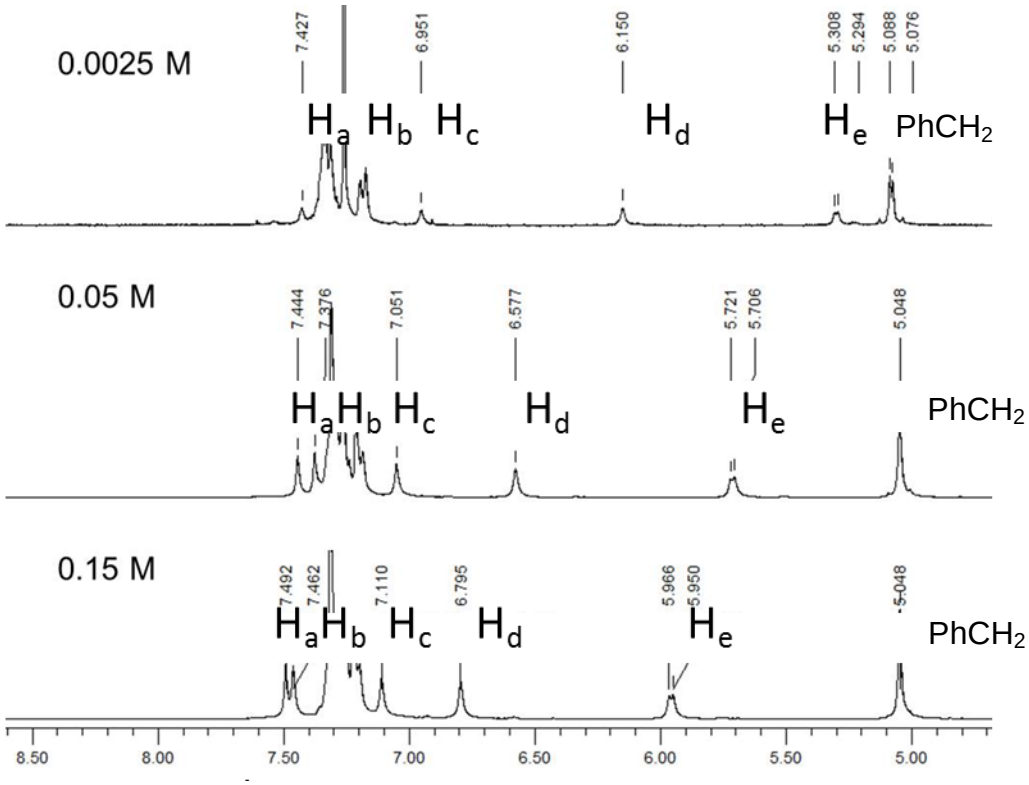

Figure S1: A graph to show a stack plot of NH shifting in Cbz-L-PheAib$_4$O^{t}Bu at different concentrations (M).

Stack Plot for Cbz-(rac)-PheAib$_4$O^{t}Bu

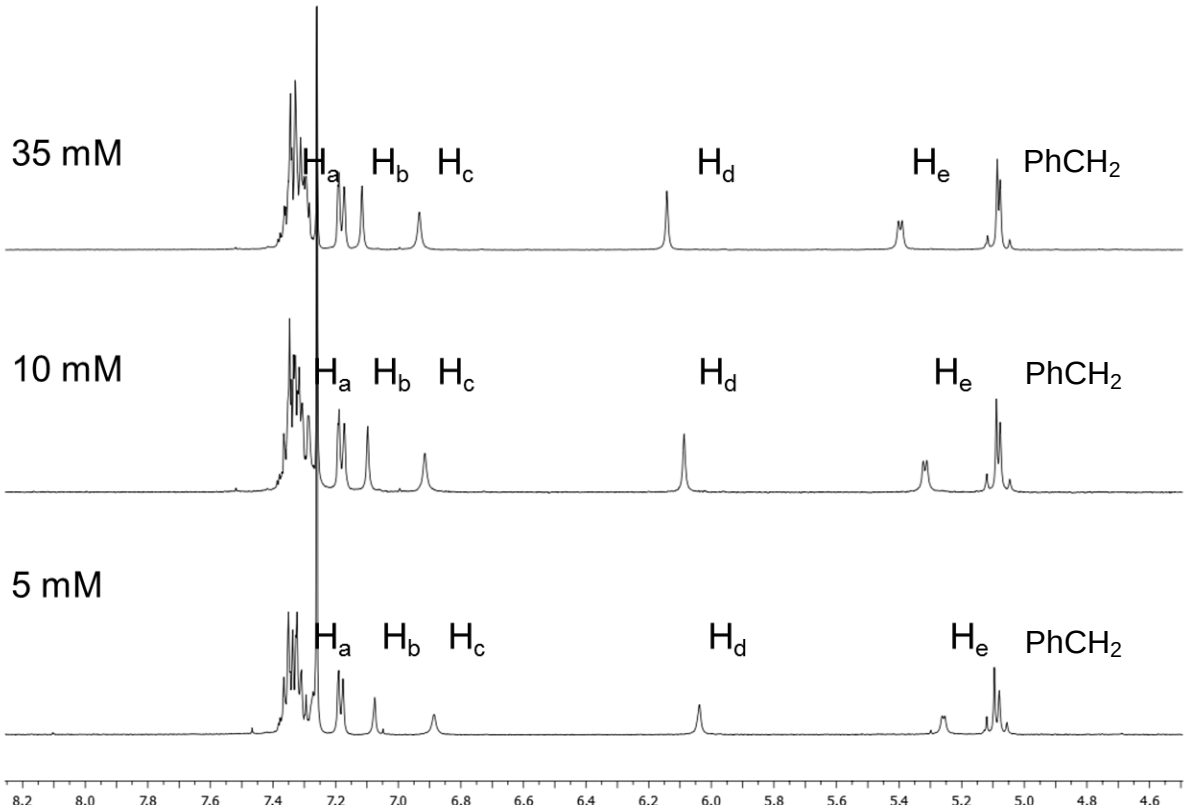

Figure S2: A graph to show a stack plot of NH shifting in Cbz-(*rac*)-PheAib$_4$O^{t}Bu at different concentrations (M).

Stack Plot for Cbz-L-(αMe)ValAib$_4$O^{t}Bu

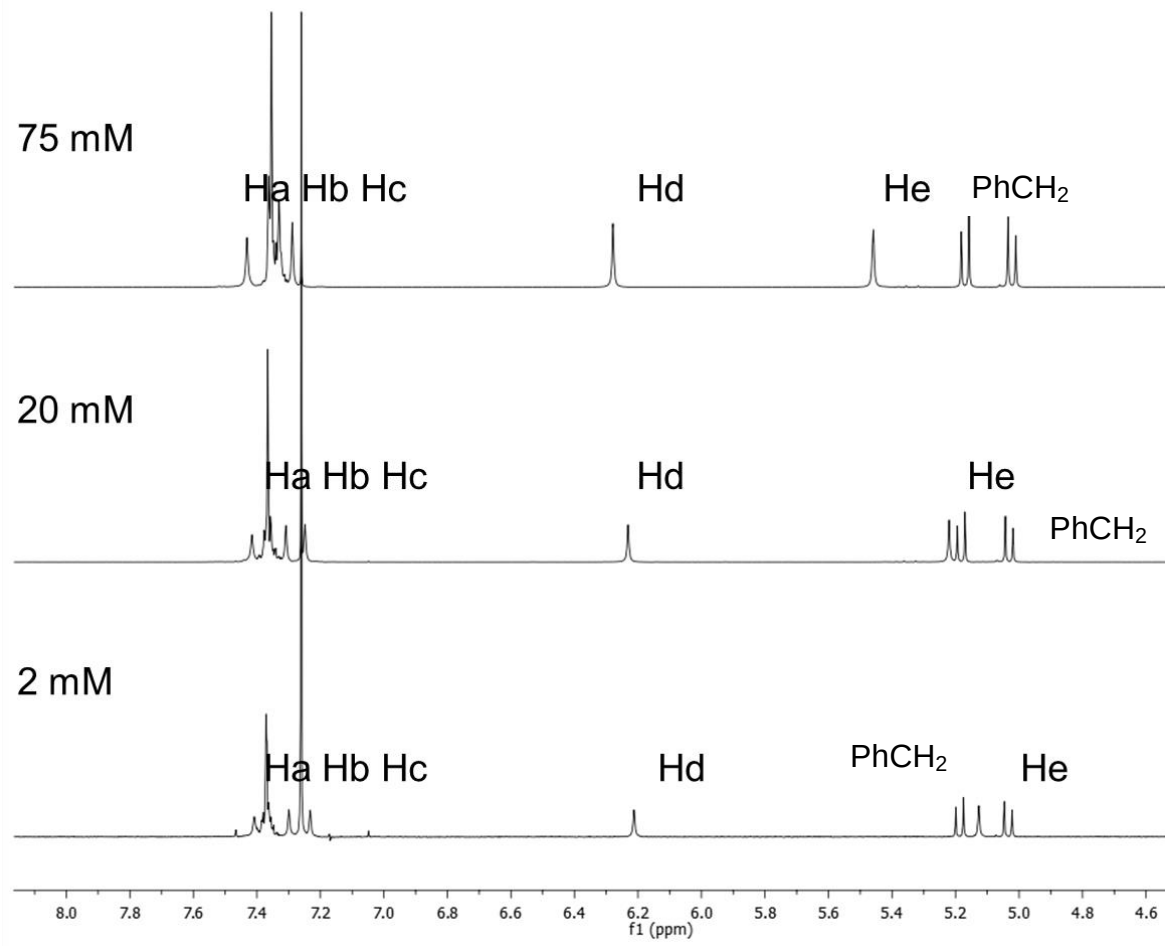

Figure S3: A graph to show a stack plot of NH shifting in Cbz-L-(αMe)ValAib$_4$O^{t}Bu at different concentrations (M).

Stack Plot for Cbz-(rac)-(αMe)ValPheAib$_4$O^{t}Bu

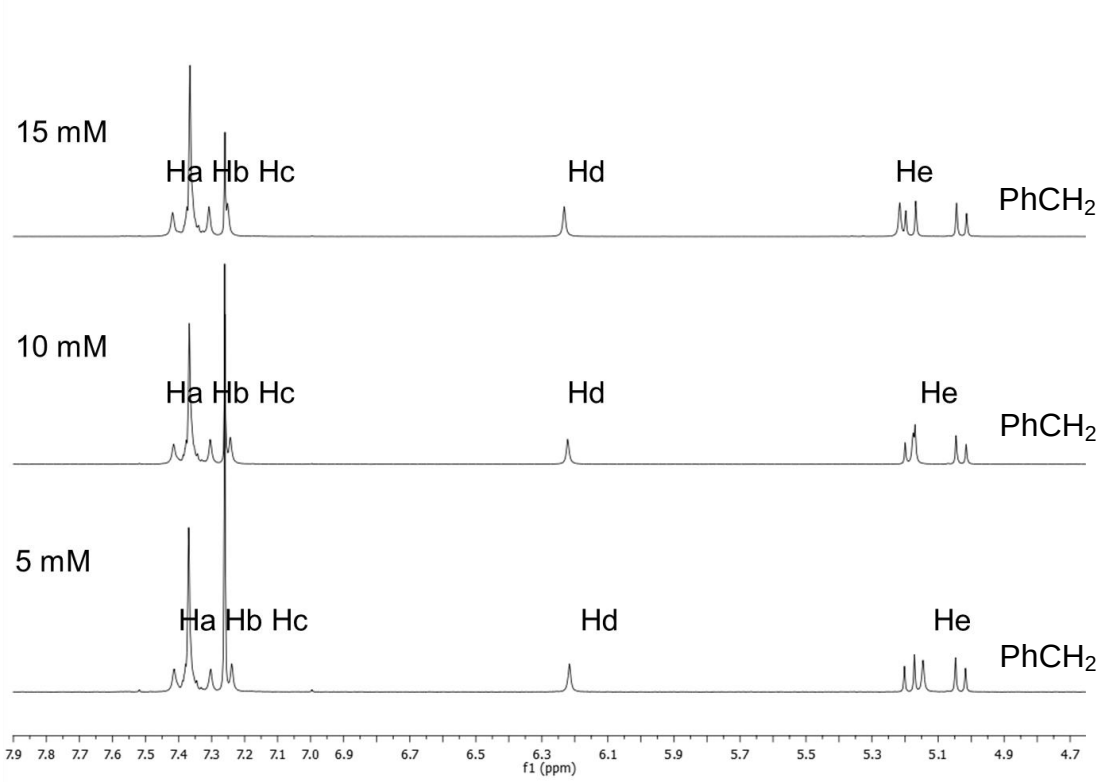

Figure S4: A graph to show a stack plot of NH shifting in Cbz-(*rac*)-(αMe)ValAib$_4$O^{t}Bu at different concentrations (M).

Calculation of dimerisation constants by iterative curve fitting

Theory

The spreadsheet macro developed by Sanderson[5] fits data to binding isotherms for the following equilibrium, using the *Solver* add-in for Excel (GRG Nonlinear Solving Method). The values obtained from this macro were verified using the same set of equations, but minimizing in SigmaPlot (Levenberg-Marquardt algorithm).

$$nH \overset{K}{\rightleftharpoons} H_n$$

where K is the microscopic association constant and ***n*** = 2.

The following equation is used to calculate the binding isotherm:

$$\delta_{obs} = \left[\frac{nK[H]^n(\delta_{bnd} - \delta_{free})}{[H]_o} \right] + \delta_{free}$$

where:

δ_{free} is the free chemical shift of the host

δ_{obs} is the observed chemical shift

δ_{bnd} is the limiting complexation-induced chemical shift change of the host in the dimeric complex

$[H]_o$ is the initial concentration of the host

[H] is the concentration of the free (uncomplexed) host

The concentration of the dimeric complex is calculated iteratively by solving the following equations:

$$[H_n] = \frac{1 + 2nK[H]_o - \sqrt{(1 + 2nK[H]_o)^2 - 4K^2n^2[H]_o^2}}{2n^2K}$$

The concentration of free host is calculated according to the concentration difference :

$$[H] = [H]_o - n[H_n]$$

In addition to the curve fits shown in the manuscript text, **Graphs S9-S12** show for each studied peptide (host in the previous equation) depicts the results obtained by this calculation method for one NH.

Iterative curve fit for Cbz-L-(αMe)ValAib$_4$O^{t}Bu (SigmaPlot)

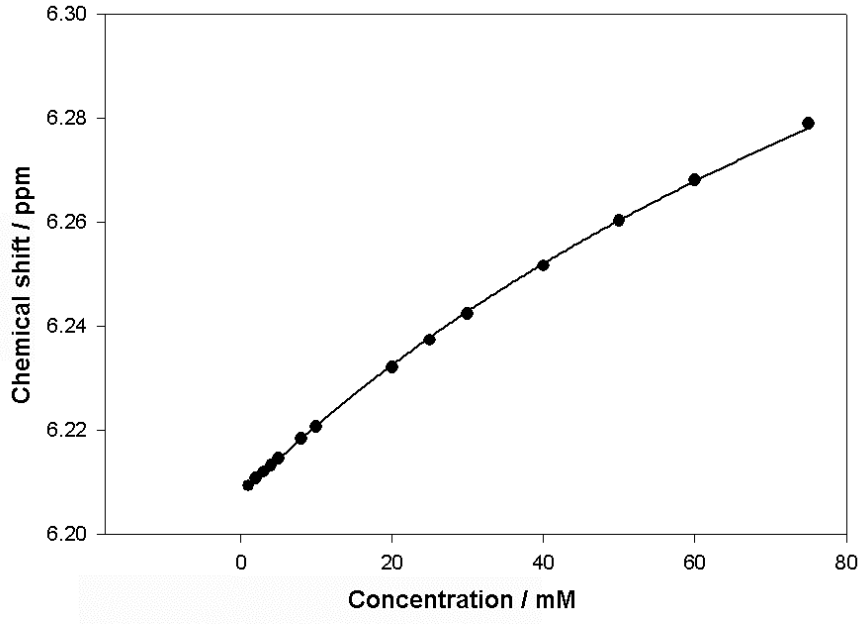

Graph S9: Plot of concentration (mM) *vs* chemical shift (ppm) for H_d in Cbz-L-(αMe)ValAib$_4$OtBu with the observed data values. Curve calculated for K = 2 M^{-1}.

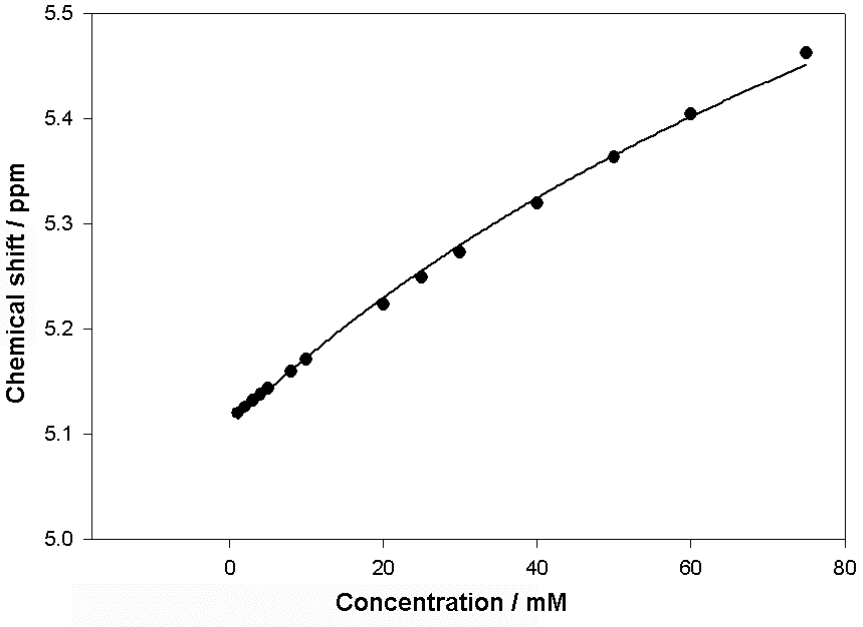

Graph S10: Plot of concentration (mM) *vs* chemical shift (ppm) for H_e in Cbz-L-(αMe)ValAib$_4$OtBu with the observed data values. Curve calculated for K = 2 M^{-1}.

Iterative curve fit for Cbz-(rac)-(αMe)ValAib$_4$O^{t}Bu (SigmaPlot)

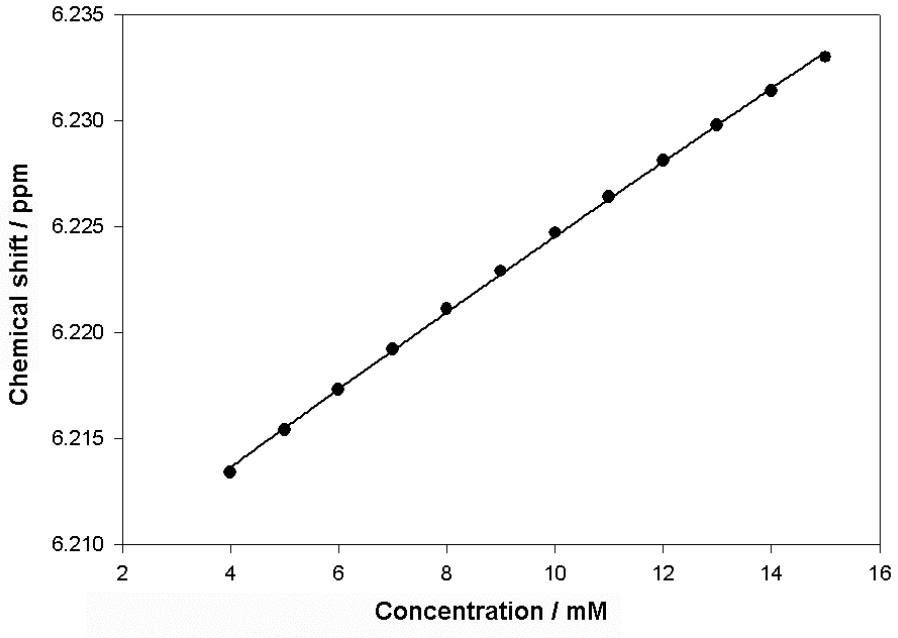

Graph S11: Plot of concentration (mM) *vs* chemical shift (ppm) for H_d in racemic Cbz-(*rac*)-(αMe)ValAib$_4$OtBu with the observed data values. Curve calculated for $K = 1\ M^{-1}$.

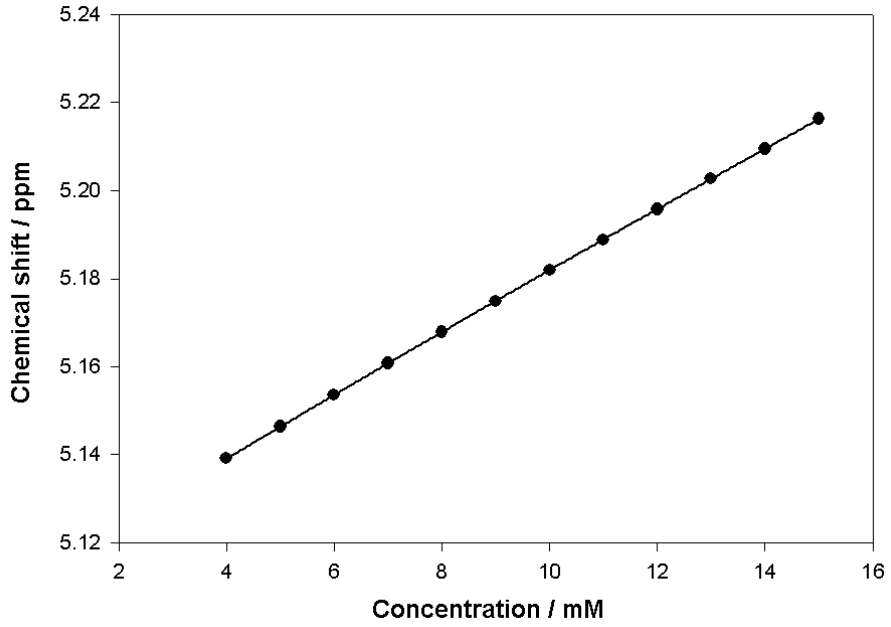

Graph S12: Plot of concentration (mM) *vs* chemical shift (ppm) for H_e in racemic Cbz-(*rac*)-(αMe)ValAib$_4$OtBu with the observed data values. Curve calculated for $K = 1\ M^{-1}$.

Calculation of dimerization constants using Huggins' dimerization model

Theory

A dimerization model of interaction between the individual oligomers was assumed to describe the aggregation of the peptides in chloroform:

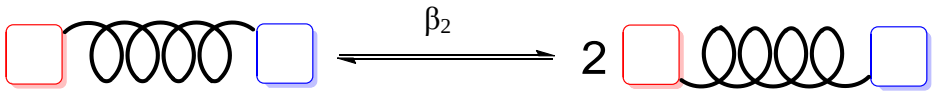

According to the Huggins' model, the constant β_2 of this equilibrium can be calculated using the following equation:

$$(\Delta\delta/\Delta[C])_{[C]=0} = 2 \times \beta_2 \times \Delta_2 = 2 \times \beta_2 \times (\Delta_s - \Delta_d)$$

where:

C is the concentration of peptide

$(\Delta\delta/\Delta[C])_{[C]=0}$ is the initial slope of the curve $\delta = f([C])$

Δ_s is the chemical shift of the unbounded peptide

Δ_d is the limiting complexation-induced chemical shift change of the peptide in the dimeric complex.

The plot of the chemical shift *vs* concentration of peptide for a given NH proton permits a value for Δ_s, Δ_d and $(\Delta\delta/\Delta[C])_{[C]=0}$ to be estimated (**Graph S13**) and a value of β_2 to be calculated. This process is repeated for each NH of the peptide and an average value of β_2 is then calculated.

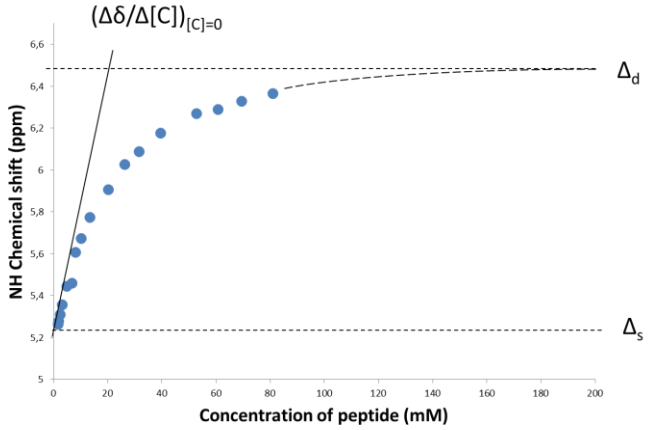

Graph S13: Graph to show the method used to estimate Δ_s, Δ_d and $(\Delta\delta/\Delta[C])_{[C]=0}$ starting from experimental data (blue dots).

Cbz-L-Phe-Aib$_4$O^{t}Bu

The equilibrium constant for H_b could not be determined because of overlapping signals in the ^{1}H NMR spectrum (aromatic protons).

	H_a	H_c	H_d	H_e	Average value
$(\Delta\delta/\Delta[C])_{[C]=0}$ ($ppm.M^{-1}$)	11.9	5.8	14.5	9.9	/
Δ_d (ppm)	7.56	7.20	6.90	5.90	/
Δ_s (ppm)	7.36	6.94	6.25	5.35	/
Equilibrium constant (M^{-1})	29.6	17.9	10.4	0.6	14.6

Table S1: Calculated equilibrium constants for each NH peak and the calculated average value obtained from the concentration studies undertaken on Cbz-L-PheAib$_4$O^{t}Bu (Figure S1 and Graph S5).

Cbz-*(rac)*-Phe-Aib$_4$O^{t}Bu

The equilibrium constant for H_a could not be determined because of overlapping signals in the ^{1}H NMR spectrum (aromatic protons).

	H_b	H_c	H_d	H_e	Average value
$(\Delta\delta/\Delta[C])_{[C]=0}$ ($ppm.M^{-1}$)	2.3	5.0	11.5	16.5	/
Δ_d (ppm)	7.17	7.05	6.55	6.30	/
Δ_s (ppm)	7.06	6.89	6.00	5.20	/
Equilibrium constant (M^{-1})	10.5	15.6	10.5	7.5	11.0

Table S2: Calculated equilibrium constants for each NH peak and the calculated average value obtained from the concentration studies undertaken on Cbz-*(rac)*-PheAib$_4$O^{t}Bu (Figure S2 and Graph S6).

Cbz-L-(αMe)Val-Aib$_4$O^{t}Bu

	H_a	H_b	H_c	H_d	H_e	Average value
$(\Delta\delta/\Delta[C])_{[C]=0}$ (ppm.M^{-1})	0.46	0.58	0.59	1.2	6.2	/
Δ_d (ppm)	7.55	7.42	7.42	6.50	6.10	/
Δ_s (ppm)	7.41	7.30	7.23	6.21	5.11	/
Equilibrium constant (M^{-1})	1.6	2.4	1.6	2.1	3.1	2.2

Table S3: Calculated equilibrium constants for each NH peak and the calculated average value obtained from the concentration studies undertaken on Cbz-L-(αMe)ValAib$_4$O^{t}Bu (Figure S3 and Graph S7).

Cbz-(*rac*)-(αMe)ValAib$_4$O^{t}Bu

The equilibrium constant for H_a could not be determined because of overlapping signals in the ^{1}H NMR spectrum (aromatic protons).

	H_a	H_b	H_c	H_d	H_e	Average value
$(\Delta\delta/\Delta[C])_{[C]=0}$ (ppm.M^{-1})	0.13	0.27	0.86	0.97	5.5	/
Δ_d (ppm)	7.45	7.40	7.38	6.50	6.80	/
Δ_s (ppm)	7.42	7.30	7.23	6.21	5.12	/
Equilibrium constant (M^{-1})	2.2	1.4	2.9	1.7	3.3	2.3

Table S4: Calculated equilibrium constants for each NH peak and the calculated average value obtained from the concentration studies undertaken on Cbz-(*rac*)-(αMe) ValAib$_4$O^{t}Bu (Figure S4 and Graph S8).

Crystal Structure Data

Cbz-(*rac*)-(αMe)ValAib$_4$O^{t}Bu

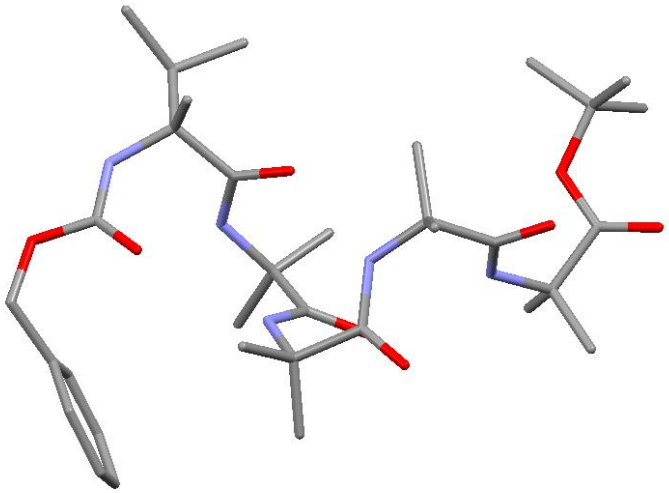

Table S5: Crystal data and structure refinement for Cbz-(*rac*)-(αMe)ValAib$_4$O^{t}Bu.

Identification code	Cbz-(*rac*)-(αMe)ValAib$_4$O^{t}Bu.	
Empirical formula	C34 H55 N5 O8	
Formula weight	661.83	
Temperature	100(2) K	
Wavelength	1.54178 Å	
Crystal system	Triclinic	
Space group	P-1	
Unit cell dimensions	a = 11.4534(8) Å	α= 96.466(5)°.
	b = 11.6801(9) Å	β= 102.806(4)°
	c = 14.4308(11) Å	γ = 90.975(4)°.
Volume	1868.8(2) Å^3	
Z	2	
Density (calculated)	1.176 Mg/m^3	
Absorption coefficient	0.684 mm^{-1}	
F(000)	716	
Crystal size	0.29 x 0.17 x 0.07 mm^3	
Theta range for data collection	3.16 to 70.15°.	
Index ranges	-13<=h<=13, -13<=k<=14, -17<=l<=16	
Reflections collected	14758	
Independent reflections	6723 [R(int) = 0.0392]	
Completeness to theta = 67.00°	95.4 %	
Absorption correction	Semi-empirical from equivalents	
Max. and min. transmission	0.9537 and 0.75506	

Refinement method	Full-matrix least-squares on F^2
Data / restraints / parameters	6723 / 2 / 472
Goodness-of-fit on F^2	1.090
Final R indices [I>2sigma(I)]	R1 = 0.0524, wR2 = 0.1417
R indices (all data)	R1 = 0.0631, wR2 = 0.1505
Largest diff. peak and hole	0.368 and -0.425 e.Å^{-3}

Table S6: Torsion angles [°] for Cbz-(*rac*)-(αMe)ValAib$_4$O^{t}Bu.

C(6)-C(1)-C(2)-C(3)	0.0
C(7)-C(1)-C(2)-C(3)	171.6(14)
C(1)-C(2)-C(3)-C(4)	0.0
C(2)-C(3)-C(4)-C(5)	0.0
C(3)-C(4)-C(5)-C(6)	0.0
C(4)-C(5)-C(6)-C(1)	0.0
C(2)-C(1)-C(6)-C(5)	0.0
C(7)-C(1)-C(6)-C(5)	-171.1(13)
C(2)-C(1)-C(7)-O(1)	143.4(15)
C(6)-C(1)-C(7)-O(1)	-45(3)
N(1)-C(9)-C(10)-C(11)	-160.38(16)
C(13)-C(9)-C(10)-C(11)	77.8(2)
C(14)-C(9)-C(10)-C(11)	-41.7(2)
N(1)-C(9)-C(10)-C(12)	74.22(19)
C(13)-C(9)-C(10)-C(12)	-47.6(2)
C(14)-C(9)-C(10)-C(12)	-167.11(16)
N(1)-C(9)-C(14)-O(3)	-146.58(18)
C(13)-C(9)-C(14)-O(3)	-25.8(3)
C(10)-C(9)-C(14)-O(3)	97.1(2)
N(1)-C(9)-C(14)-N(2)	34.9(2)
C(13)-C(9)-C(14)-N(2)	155.71(19)
C(10)-C(9)-C(14)-N(2)	-81.4(2)
N(2)-C(15)-C(18)-O(4)	-153.71(18)
C(16)-C(15)-C(18)-O(4)	-31.6(2)
C(17)-C(15)-C(18)-O(4)	89.2(2)
N(2)-C(15)-C(18)-N(3)	28.2(2)
C(16)-C(15)-C(18)-N(3)	150.32(18)

C(17)-C(15)-C(18)-N(3)	-88.8(2)
N(3)-C(19)-C(22)-O(5)	-150.65(17)
C(20)-C(19)-C(22)-O(5)	-27.6(2)
C(21)-C(19)-C(22)-O(5)	93.1(2)
N(3)-C(19)-C(22)-N(4)	34.0(2)
C(20)-C(19)-C(22)-N(4)	157.06(16)
C(21)-C(19)-C(22)-N(4)	-82.28(19)
N(4)-C(23)-C(26)-O(6)	-164.83(16)
C(24)-C(23)-C(26)-O(6)	77.94(19)
C(25)-C(23)-C(26)-O(6)	-40.7(2)
N(4)-C(23)-C(26)-N(5)	22.1(2)
C(24)-C(23)-C(26)-N(5)	-95.17(19)
C(25)-C(23)-C(26)-N(5)	146.23(18)
N(5)-C(27)-C(30)-O(7)	135.31(17)
C(29)-C(27)-C(30)-O(7)	12.8(2)
C(28)-C(27)-C(30)-O(7)	-107.42(19)
N(5)-C(27)-C(30)-O(8)	-49.13(18)
C(29)-C(27)-C(30)-O(8)	-171.66(14)
C(28)-C(27)-C(30)-O(8)	68.14(18)
O(2)-C(8)-N(1)-C(9)	-3.7(3)
O(1)-C(8)-N(1)-C(9)	177.10(16)
C(13)-C(9)-N(1)-C(8)	-63.1(2)
C(14)-C(9)-N(1)-C(8)	55.9(2)
C(10)-C(9)-N(1)-C(8)	173.65(17)
O(3)-C(14)-N(2)-C(15)	-2.0(3)
C(9)-C(14)-N(2)-C(15)	176.48(18)
C(16)-C(15)-N(2)-C(14)	-66.9(2)
C(17)-C(15)-N(2)-C(14)	171.76(18)
C(18)-C(15)-N(2)-C(14)	54.8(2)
O(4)-C(18)-N(3)-C(19)	1.3(3)
C(15)-C(18)-N(3)-C(19)	179.27(17)
C(20)-C(19)-N(3)-C(18)	-71.4(2)
C(21)-C(19)-N(3)-C(18)	167.68(19)
C(22)-C(19)-N(3)-C(18)	52.1(2)
O(5)-C(22)-N(4)-C(23)	-1.2(3)
C(19)-C(22)-N(4)-C(23)	174.06(15)
C(24)-C(23)-N(4)-C(22)	179.54(16)
C(26)-C(23)-N(4)-C(22)	63.7(2)

C(25)-C(23)-N(4)-C(22)	-60.2(2)
O(6)-C(26)-N(5)-C(27)	0.9(3)
C(23)-C(26)-N(5)-C(27)	173.87(16)
C(29)-C(27)-N(5)-C(26)	72.7(2)
C(28)-C(27)-N(5)-C(26)	-166.07(17)
C(30)-C(27)-N(5)-C(26)	-49.3(2)
O(2)-C(8)-O(1)-C(7)	-0.2(6)
N(1)-C(8)-O(1)-C(7)	179.0(5)
O(2)-C(8)-O(1)-C(7S)	-10.2(7)
N(1)-C(8)-O(1)-C(7S)	169.0(6)
C(1)-C(7)-O(1)-C(8)	-62(2)
C(1)-C(7)-O(1)-C(7S)	15(17)
O(7)-C(30)-O(8)-C(31)	-2.8(3)
C(27)-C(30)-O(8)-C(31)	-178.32(14)
C(34)-C(31)-O(8)-C(30)	-178.77(18)
C(32)-C(31)-O(8)-C(30)	63.9(3)
C(33)-C(31)-O(8)-C(30)	-60.2(3)
C(6S)-C(1S)-C(2S)-C(3S)	0.0
C(7S)-C(1S)-C(2S)-C(3S)	-174.6(10)
C(1S)-C(2S)-C(3S)-C(4S)	0.0
C(2S)-C(3S)-C(4S)-C(5S)	0.0
C(3S)-C(4S)-C(5S)-C(6S)	0.0
C(4S)-C(5S)-C(6S)-C(1S)	0.0
C(2S)-C(1S)-C(6S)-C(5S)	0.0
C(7S)-C(1S)-C(6S)-C(5S)	174.8(11)
C(8)-O(1)-C(7S)-C(1S)	-80(3)
C(7)-O(1)-C(7S)-C(1S)	172(21)
C(2S)-C(1S)-C(7S)-O(1)	128.4(19)
C(6S)-C(1S)-C(7S)-O(1)	-46(3)

Table S7: Hydrogen bonds for Cbz-(*rac*)-(αMe)ValAib$_4$O^{t}Bu. [Å and °].

D-H...A	d(D-H)	d(H...A)	d(D...A)	<(DHA)
N(1)-H(1)...O(6)#1	0.88	2.02	2.863(2)	160.3
N(3)-H(3A)...O(2)	0.88	2.20	3.030(2)	157.0
N(4)-H(4A)...O(3)	0.88	2.12	2.9588(19)	159.9
N(5)-H(5A)...O(4)	0.88	2.17	3.033(2)	165.9

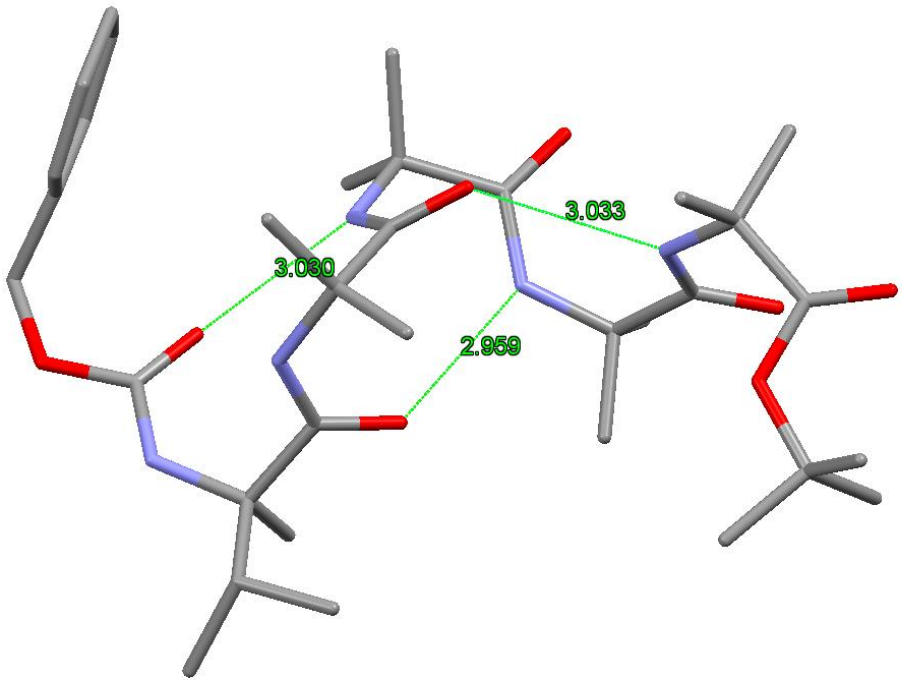

Figure S5: Intramolecular hydrogen bonding interactions present in Cbz-(*rac*)-(αMe)ValAibO^{t}Bu.

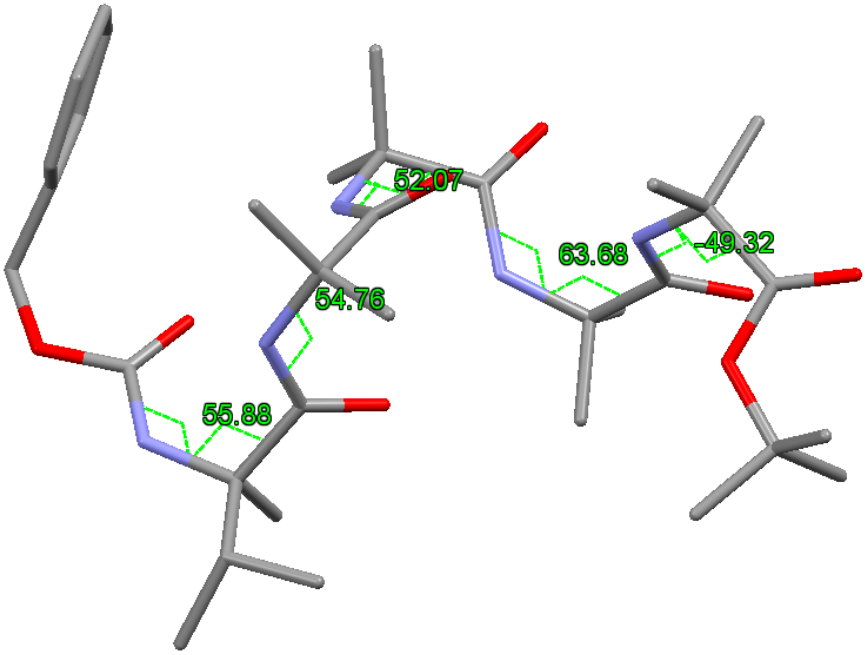

Figure S6: ψ torsion angles present in Cbz-(*rac*)-(αMe)ValAib$_4$O^{t}Bu.

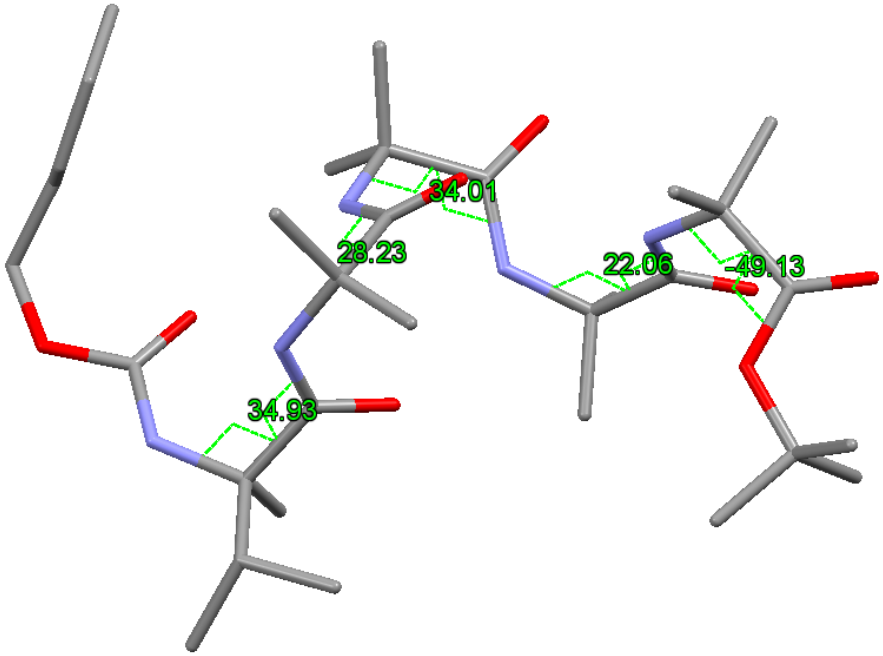

Figure S7: ϕ torsion angles present in Cbz-(*rac*)-(αMe)ValAib$_4$O^{t}Bu.

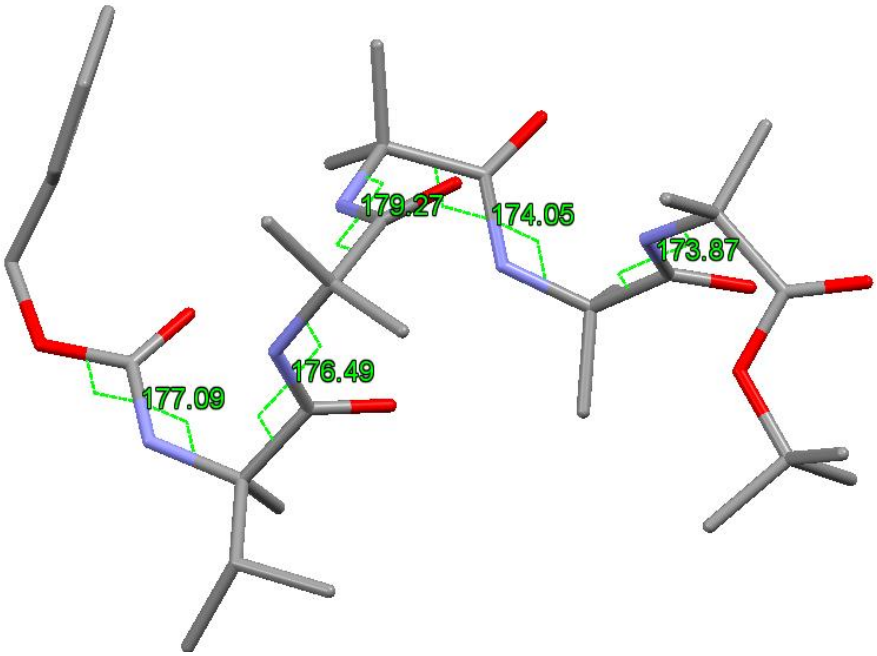

Figure S8: ω torsion angles present in Cbz-(*rac*)-(αMe)ValAib$_4$O^{t}Bu.

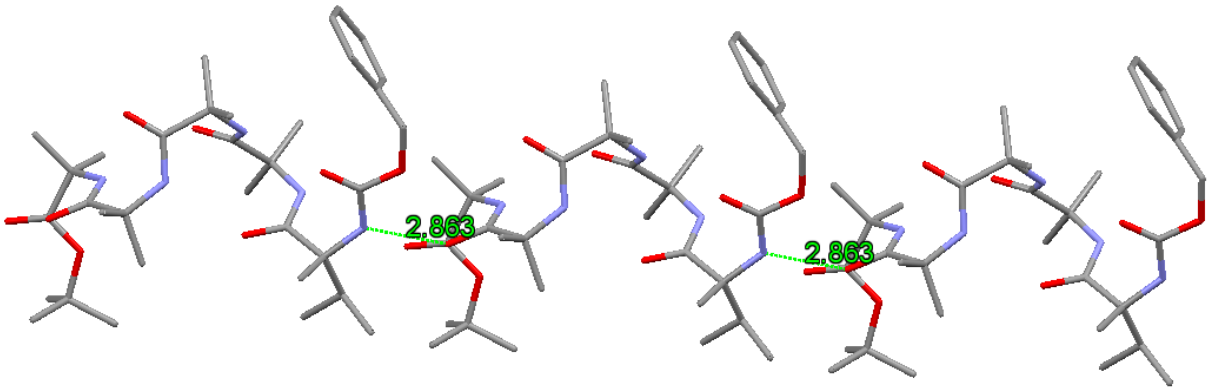

Figure S9: Intermolecular hydrogen bonding interactions present in Cbz-(*rac*)-(αMe)ValAib$_4$O^{t}Bu.

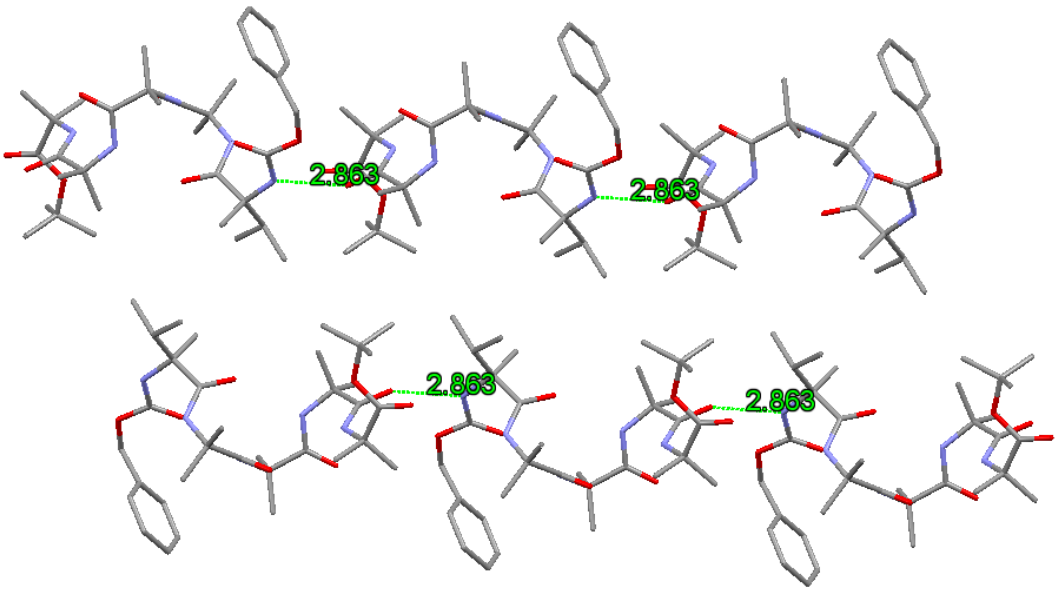

Figure S10: Intermolecular hydrogen bonding interactions present and the crystal packing in Cbz-(*rac*)-(αMe)ValAib$_4$O^{t}Bu.

Crystal Structure Data

Cbz-(*rac*)-PheAib$_4$O^{t}Bu (reported in reference 8)

Table S8. Crystal data and structure refinement for Cbz-(*rac*)-PheAib$_4$O^{t}Bu.

Identification code	Cbz-(*rac*)-PheAib$_4$O^{t}Bu.	
Empirical formula	C39 H55 Cl6 N5 O8	
Formula weight	934.58	
Temperature	100(2) K	
Wavelength	1.54178 Å	
Crystal system	Triclinic	
Space group	P-1	
Unit cell dimensions	a = 11.3070(4) Å	α= 70.683(2)°.
	b = 13.8002(4) Å	β= 73.734(2)°.
	c = 17.3410(5) Å	γ = 71.237(2)°.
Volume	2371.72(13) Å^3	
Z	2	
Density (calculated)	1.309 Mg/m^3	
Absorption coefficient	3.734 mm^{-1}	
F(000)	980	
Crystal size	0.29 x 0.17 x 0.08 mm^3	
Theta range for data collection	2.75 to 69.95°.	
Index ranges	-13<=h<=12, -16<=k<=16, -21<=l<=20	
Reflections collected	18687	
Independent reflections	8514 [R(int) = 0.0380]	
Completeness to theta = 67.00°	95.7 %	
Absorption correction	Semi-empirical from equivalents	
Max. and min. transmission	0.7544 and 0.497525	
Refinement method	Full-matrix least-squares on F^2	
Data / restraints / parameters	8514 / 10 / 554	
Goodness-of-fit on F^2	1.070	
Final R indices [I>2sigma(I)]	R1 = 0.0659, wR2 = 0.1562	
R indices (all data)	R1 = 0.0815, wR2 = 0.1683	
Largest diff. peak and hole	1.111 and -0.835 e.Å^{-3}	

Table S9: Torsion angles [°] for Cbz-(*rac*)-PheAib$_4$O^{t}Bu.

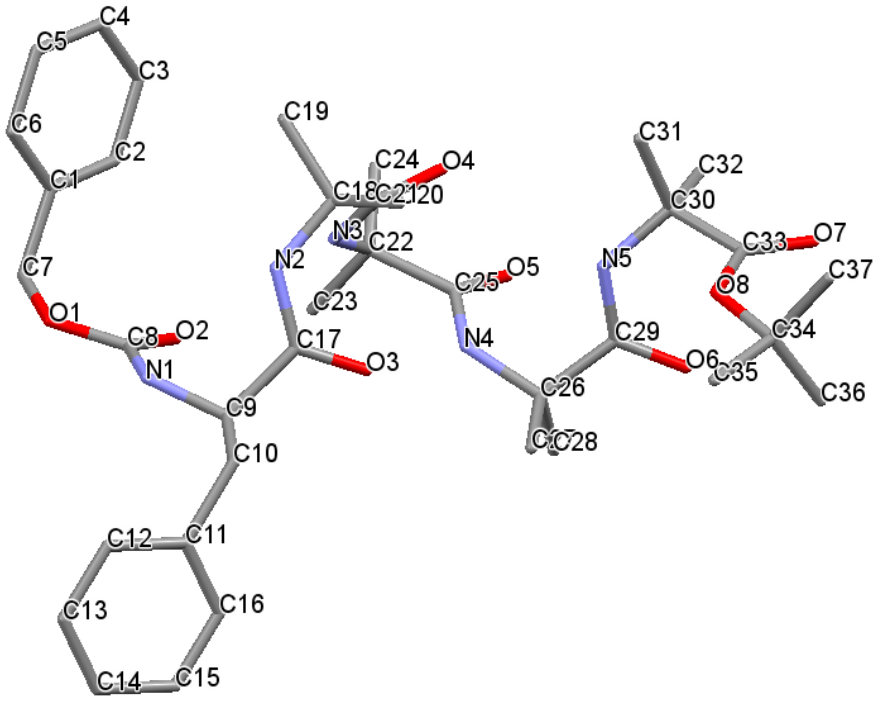

C(6)-C(1)-C(2)-C(3)	0.1(5)
C(7)-C(1)-C(2)-C(3)	-178.5(3)
C(1)-C(2)-C(3)-C(4)	-0.6(6)
C(2)-C(3)-C(4)-C(5)	0.9(6)
C(3)-C(4)-C(5)-C(6)	-0.7(6)
C(4)-C(5)-C(6)-C(1)	0.2(6)
C(2)-C(1)-C(6)-C(5)	0.1(5)
C(7)-C(1)-C(6)-C(5)	178.7(3)
C(2)-C(1)-C(7)-O(1)	-106.5(4)
C(6)-C(1)-C(7)-O(1)	75.0(4)
N(1)-C(9)-C(10)-C(11)	-75.5(4)
C(17)-C(9)-C(10)-C(11)	165.5(3)
C(9)-C(10)-C(11)-C(12)	97.2(4)
C(9)-C(10)-C(11)-C(16)	-80.5(4)
C(16)-C(11)-C(12)-C(13)	0.0
C(10)-C(11)-C(12)-C(13)	-177.7(4)
C(11)-C(12)-C(13)-C(14)	0.0
C(12)-C(13)-C(14)-C(15)	0.0
C(13)-C(14)-C(15)-C(16)	0.0
C(14)-C(15)-C(16)-C(11)	0.0
C(12)-C(11)-C(16)-C(15)	0.0

C(10)-C(11)-C(16)-C(15)	177.7(4)
C(17)-C(9S)-C(10S)-C(11S)	-173.7(8)
N(1)-C(9S)-C(10S)-C(11S)	72.0(10)
C(9S)-C(10S)-C(11S)-C(12S)	-5.6(12)
C(9S)-C(10S)-C(11S)-C(16S)	179.4(8)
C(16S)-C(11S)-C(12S)-C(13S)	0.0
C(10S)-C(11S)-C(12S)-C(13S)	-174.9(11)
C(11S)-C(12S)-C(13S)-C(14S)	0.0
C(12S)-C(13S)-C(14S)-C(15S)	0.0
C(13S)-C(14S)-C(15S)-C(16S)	0.0
C(14S)-C(15S)-C(16S)-C(11S)	0.0
C(12S)-C(11S)-C(16S)-C(15S)	0.0
C(10S)-C(11S)-C(16S)-C(15S)	175.2(10)
C(10S)-C(9S)-C(17)-O(3)	27.1(10)
N(1)-C(9S)-C(17)-O(3)	140.1(5)
C(10S)-C(9S)-C(17)-N(2)	-170.6(6)
N(1)-C(9S)-C(17)-N(2)	-57.6(8)
C(10S)-C(9S)-C(17)-C(9)	-48.5(10)
N(1)-C(9S)-C(17)-C(9)	64.6(10)
N(1)-C(9)-C(17)-O(3)	161.3(3)
C(10)-C(9)-C(17)-O(3)	-80.5(4)
N(1)-C(9)-C(17)-N(2)	-12.7(5)
C(10)-C(9)-C(17)-N(2)	105.6(4)
N(1)-C(9)-C(17)-C(9S)	-80.0(11)
C(10)-C(9)-C(17)-C(9S)	38.2(10)
N(2)-C(18)-C(21)-O(4)	155.8(3)
C(20)-C(18)-C(21)-O(4)	33.1(4)
C(19)-C(18)-C(21)-O(4)	-87.7(3)
N(2)-C(18)-C(21)-N(3)	-25.2(4)
C(20)-C(18)-C(21)-N(3)	-147.9(3)
C(19)-C(18)-C(21)-N(3)	91.3(3)
N(3)-C(22)-C(25)-O(5)	150.1(3)
C(24)-C(22)-C(25)-O(5)	26.5(4)
C(23)-C(22)-C(25)-O(5)	-93.7(3)
N(3)-C(22)-C(25)-N(4)	-33.7(3)
C(24)-C(22)-C(25)-N(4)	-157.2(2)
C(23)-C(22)-C(25)-N(4)	82.5(3)
N(4)-C(26)-C(29)-O(6)	160.8(3)

C(28)-C(26)-C(29)-O(6)	37.5(4)
C(27)-C(26)-C(29)-O(6)	-82.0(3)
N(4)-C(26)-C(29)-N(5)	-25.3(4)
C(28)-C(26)-C(29)-N(5)	-148.6(3)
C(27)-C(26)-C(29)-N(5)	91.9(3)
N(5)-C(30)-C(33)-O(7)	-137.3(3)
C(32)-C(30)-C(33)-O(7)	-15.0(4)
C(31)-C(30)-C(33)-O(7)	105.8(3)
N(5)-C(30)-C(33)-O(8)	48.0(3)
C(32)-C(30)-C(33)-O(8)	170.3(2)
C(31)-C(30)-C(33)-O(8)	-69.0(3)
O(2)-C(8)-N(1)-C(9)	8.3(5)
O(1)-C(8)-N(1)-C(9)	-172.6(3)
O(2)-C(8)-N(1)-C(9S)	-13.1(8)
O(1)-C(8)-N(1)-C(9S)	166.0(6)
C(10)-C(9)-N(1)-C(8)	170.8(3)
C(17)-C(9)-N(1)-C(8)	-71.9(4)
C(10)-C(9)-N(1)-C(9S)	-50.3(10)
C(17)-C(9)-N(1)-C(9S)	67.0(11)
C(17)-C(9S)-N(1)-C(8)	-24.8(10)
C(10S)-C(9S)-N(1)-C(8)	83.7(8)
C(17)-C(9S)-N(1)-C(9)	-78.0(11)
C(10S)-C(9S)-N(1)-C(9)	30.6(8)
O(3)-C(17)-N(2)-C(18)	-1.4(5)
C(9S)-C(17)-N(2)-C(18)	-164.5(5)
C(9)-C(17)-N(2)-C(18)	172.2(3)
C(20)-C(18)-N(2)-C(17)	67.4(4)
C(19)-C(18)-N(2)-C(17)	-171.9(3)
C(21)-C(18)-N(2)-C(17)	-54.9(4)
O(4)-C(21)-N(3)-C(22)	-5.0(4)
C(18)-C(21)-N(3)-C(22)	176.0(3)
C(24)-C(22)-N(3)-C(21)	70.3(3)
C(23)-C(22)-N(3)-C(21)	-168.3(3)
C(25)-C(22)-N(3)-C(21)	-52.5(3)
O(5)-C(25)-N(4)-C(26)	1.2(4)
C(22)-C(25)-N(4)-C(26)	-175.0(2)
C(28)-C(26)-N(4)-C(25)	61.5(3)
C(27)-C(26)-N(4)-C(25)	-177.3(2)

C(29)-C(26)-N(4)-C(25)	-61.4(3)
O(6)-C(29)-N(5)-C(30)	-8.5(4)
C(26)-C(29)-N(5)-C(30)	177.6(2)
C(32)-C(30)-N(5)-C(29)	-72.9(3)
C(33)-C(30)-N(5)-C(29)	49.7(4)
C(31)-C(30)-N(5)-C(29)	166.7(3)
O(2)-C(8)-O(1)-C(7)	6.0(5)
N(1)-C(8)-O(1)-C(7)	-173.1(3)
C(1)-C(7)-O(1)-C(8)	78.6(4)
O(7)-C(33)-O(8)-C(34)	4.3(5)
C(30)-C(33)-O(8)-C(34)	178.9(2)
C(35)-C(34)-O(8)-C(33)	175.7(3)
C(36)-C(34)-O(8)-C(33)	57.3(4)
C(37)-C(34)-O(8)-C(33)	-66.4(4)

Table S10: Hydrogen bonds for Cbz-(*rac*)-PheAib$_4$O^{t}Bu [Å and °].

D-H...A	d(D-H)	d(H...A)	d(D...A)	<(DHA)
N(5)-H(5A)...O(4)	0.88	2.24	3.058(3)	153.9
N(1)-H(1)...O(6)#1	0.88	1.95	2.801(4)	163.4
N(3)-H(3A)...O(2)	0.88	2.21	3.054(3)	161.7
N(4)-H(4A)...O(3)	0.88	2.04	2.889(3)	160.6

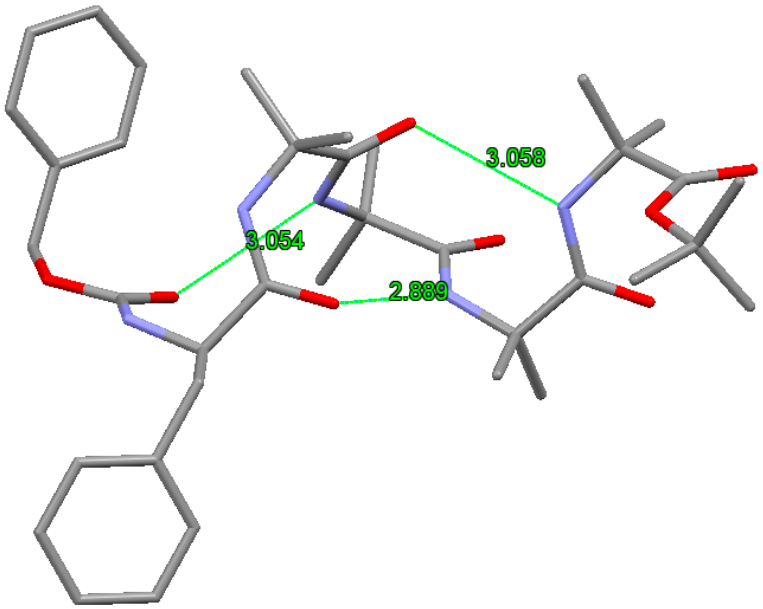

Figure S11: Intramolecular hydrogen bonding interactions present in Cbz-(*rac*)-PheAib$_4$O^{t}Bu.

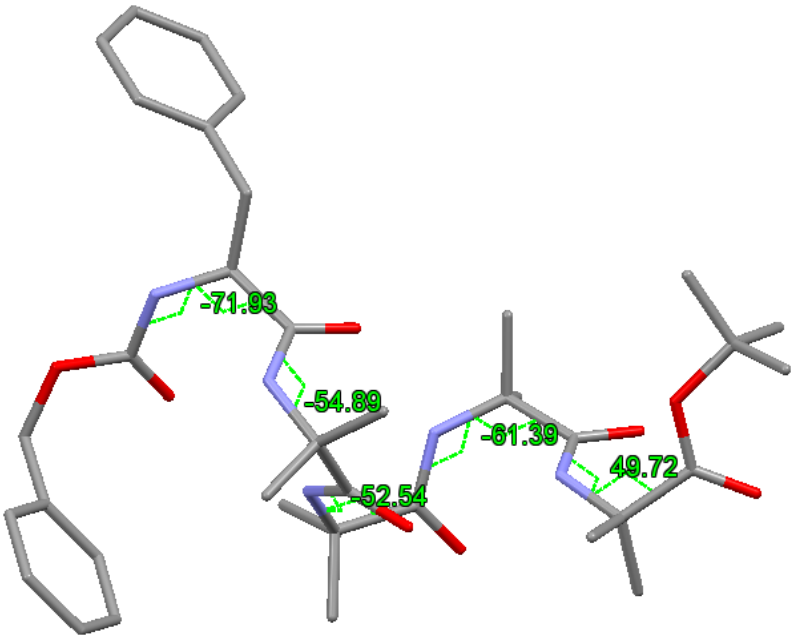

Figure S12: ϕ torsion angles present in Cbz-(*rac*)-PheAib$_4$O^{t}Bu.

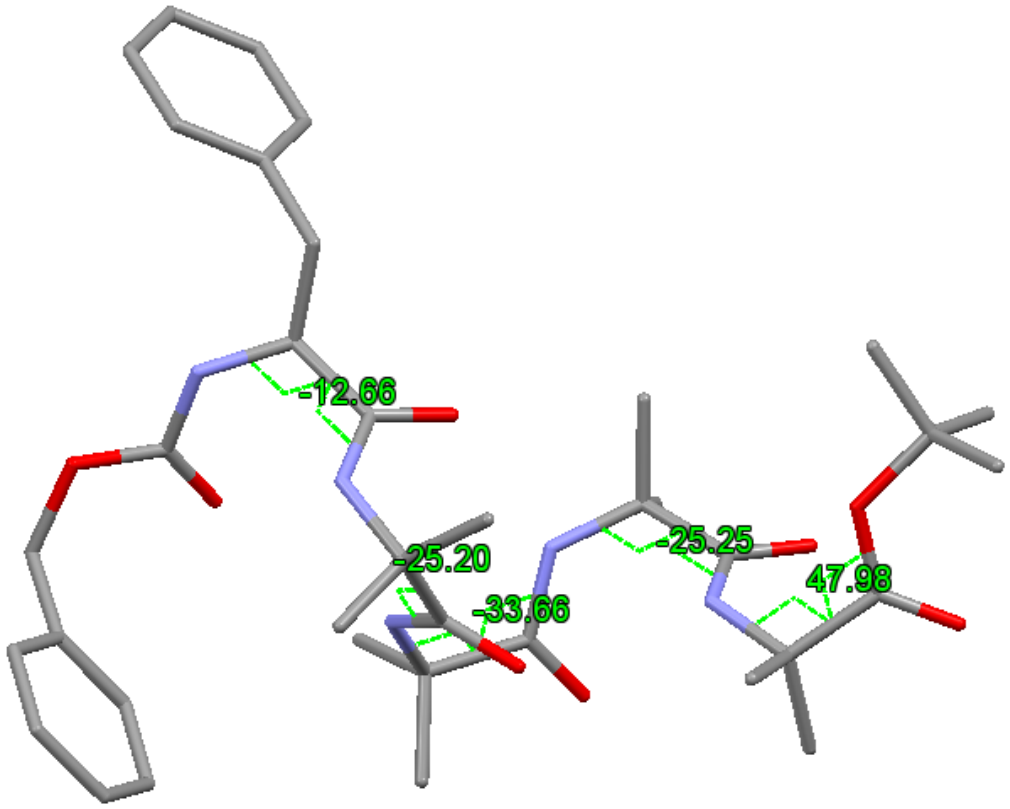

Figure S13: ψ torsion angles present in Cbz-(*rac*)-PheAib$_4$O^{t}Bu.

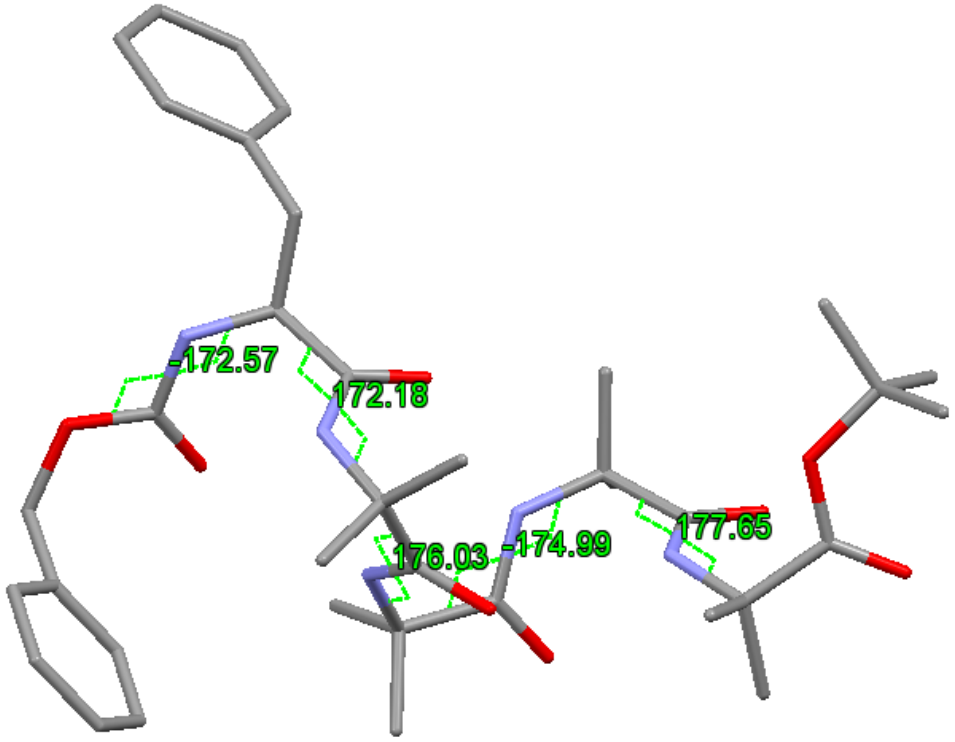

Figure S14: ω torsion angles present in Cbz-(*rac*)-PheAib$_4$O^{t}Bu.

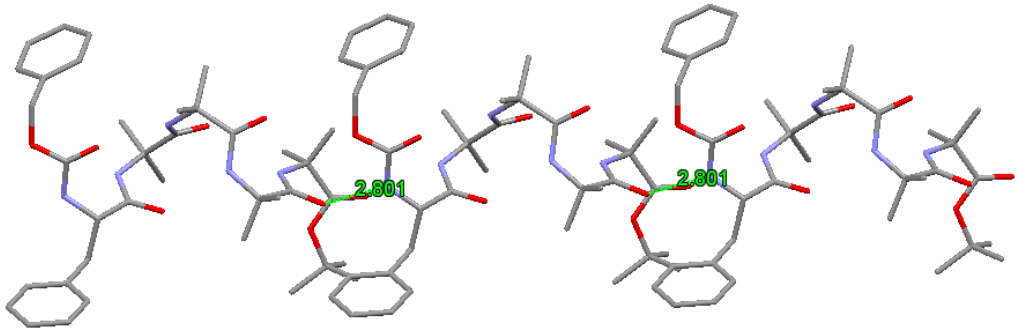

Figure S15: Intermolecular hydrogen bonding interactions present in Cbz-(*rac*)-Phe-Aib_4O^tBu.

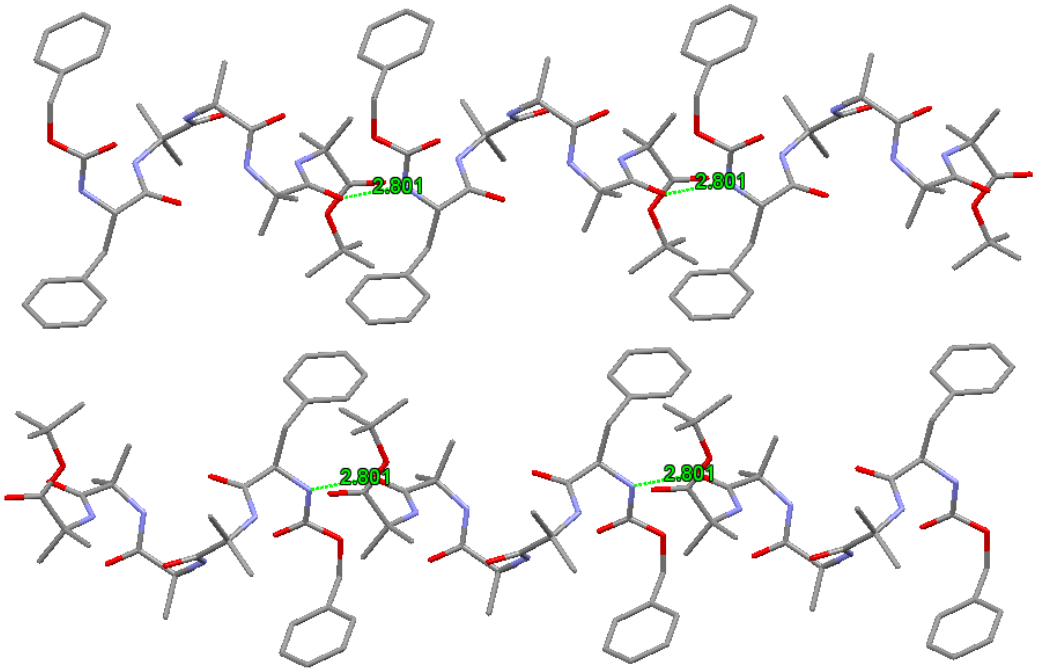

Figure S16: Intermolecular hydrogen bonding interactions and crystal packing present in Cbz-(*rac*)-PheAib_4O^tBu.

Appendix A: ^{1}H, ^{13}C NMR spectra of compounds

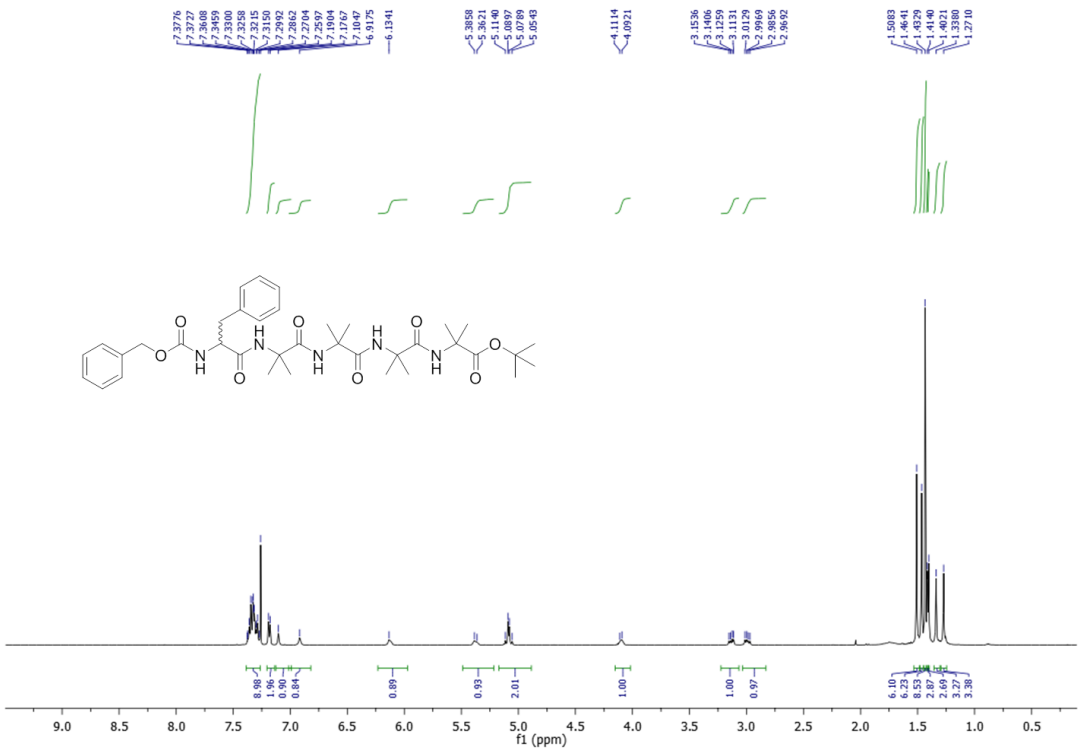

^{1}H NMR spectrum (500 MHz, $CDCl_3$) of Cbz-(*rac*)-PheAib$_4$O^{t}Bu.

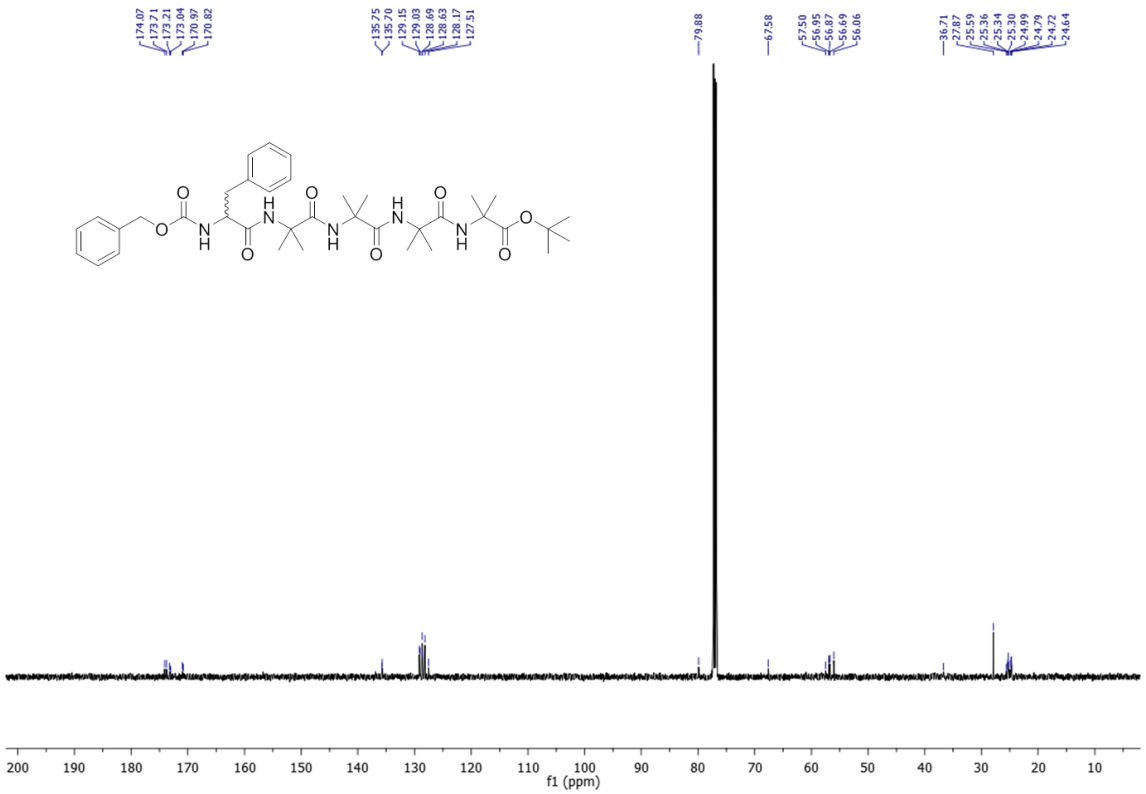

^{13}C NMR spectrum (125 MHz, $CDCl_3$) of Cbz-(*rac*)-PheAib$_4$O^{t}Bu.

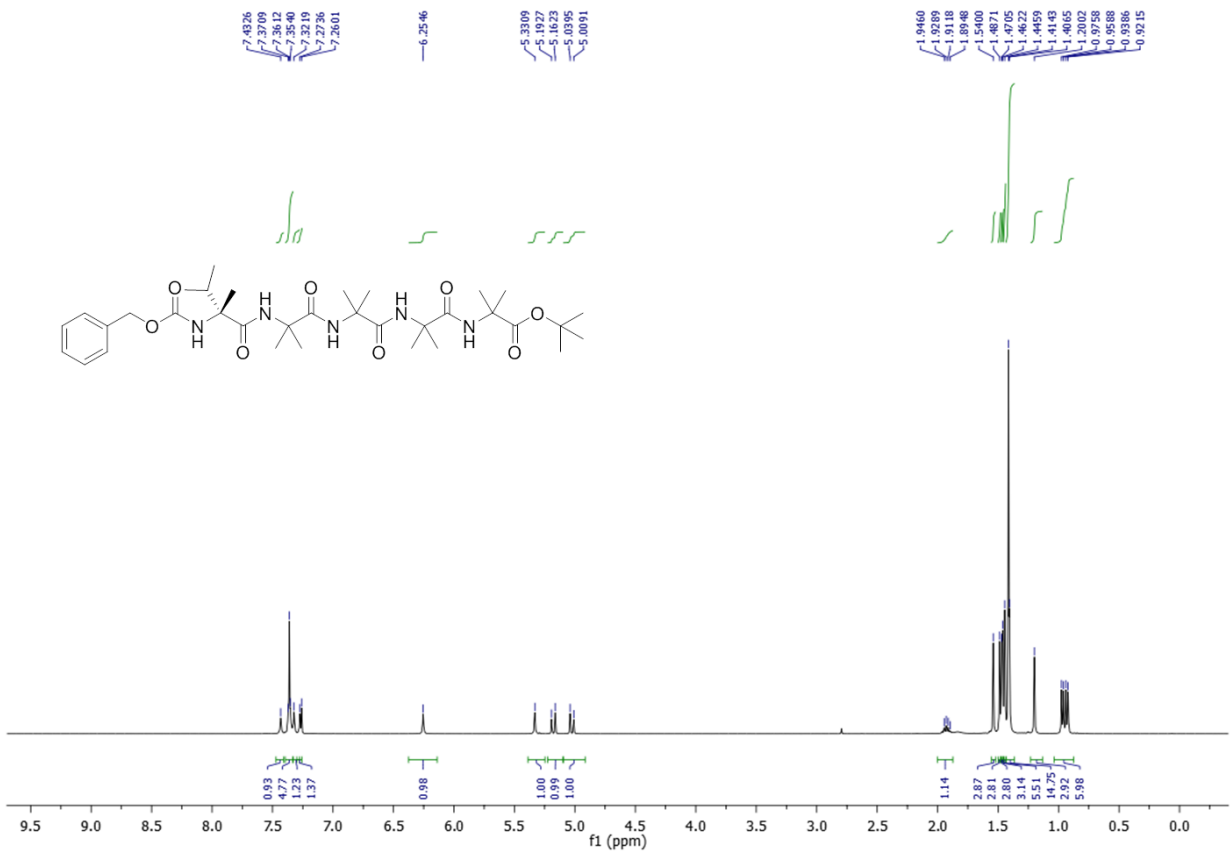

^{1}H NMR spectrum (500 MHz, $CDCl_3$) of Cbz-D-(αMe)ValAib$_4$O^{t}Bu.

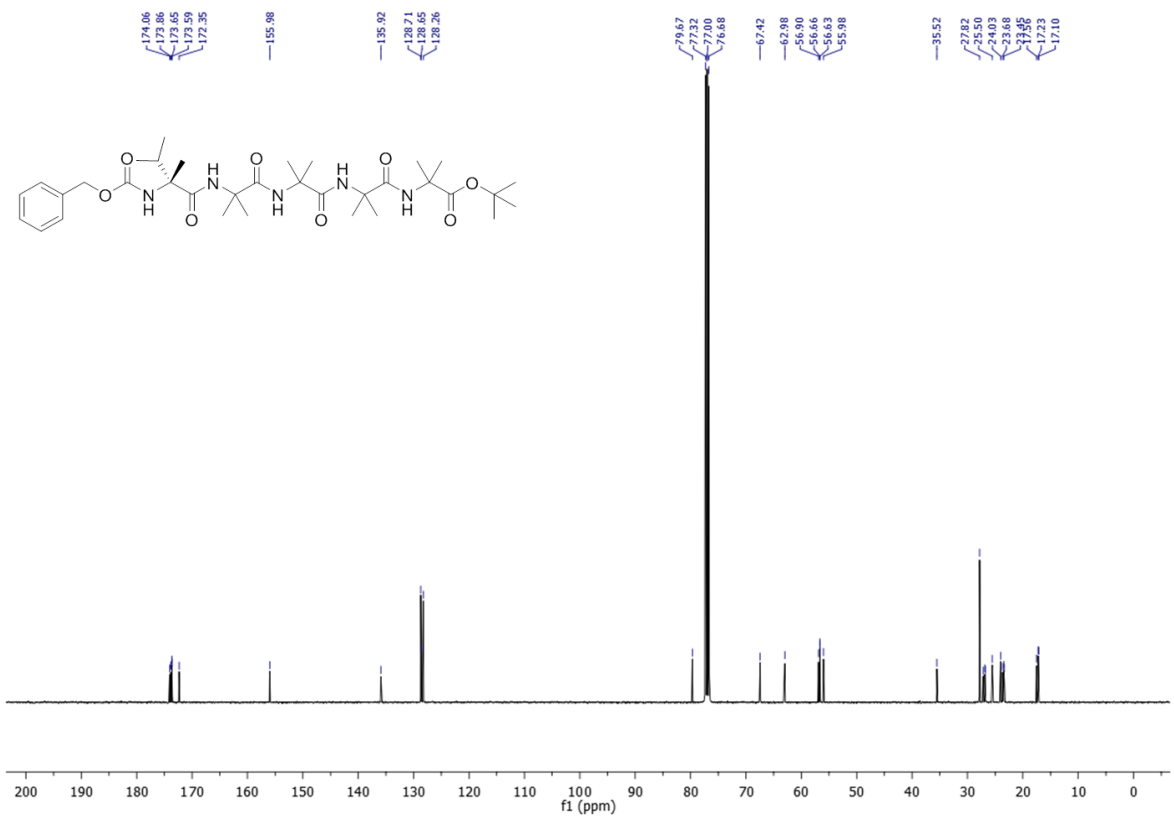

^{13}C NMR spectrum (75 MHz, $CDCl_3$) of Cbz-D-(αMe)ValAib$_4$O^{t}Bu.

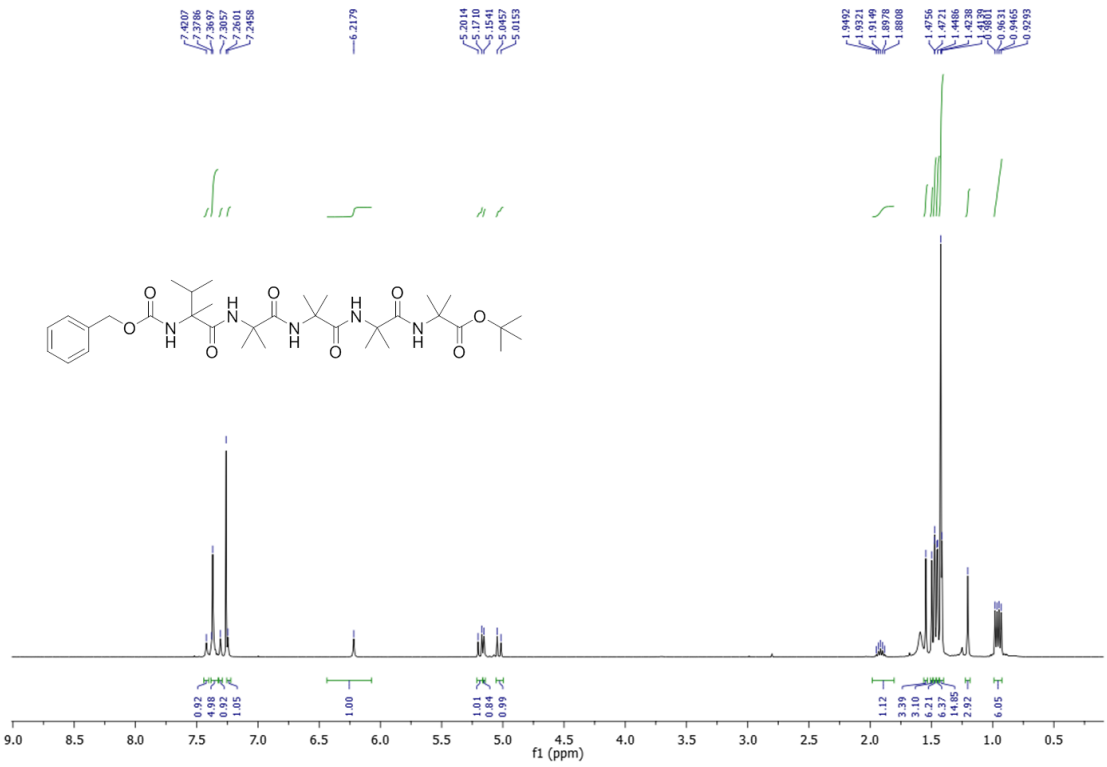

^{1}H NMR spectrum (400 MHz, $CDCl_3$) of Cbz-(*rac*)-(αMe)ValAib$_4$O^{t}Bu.

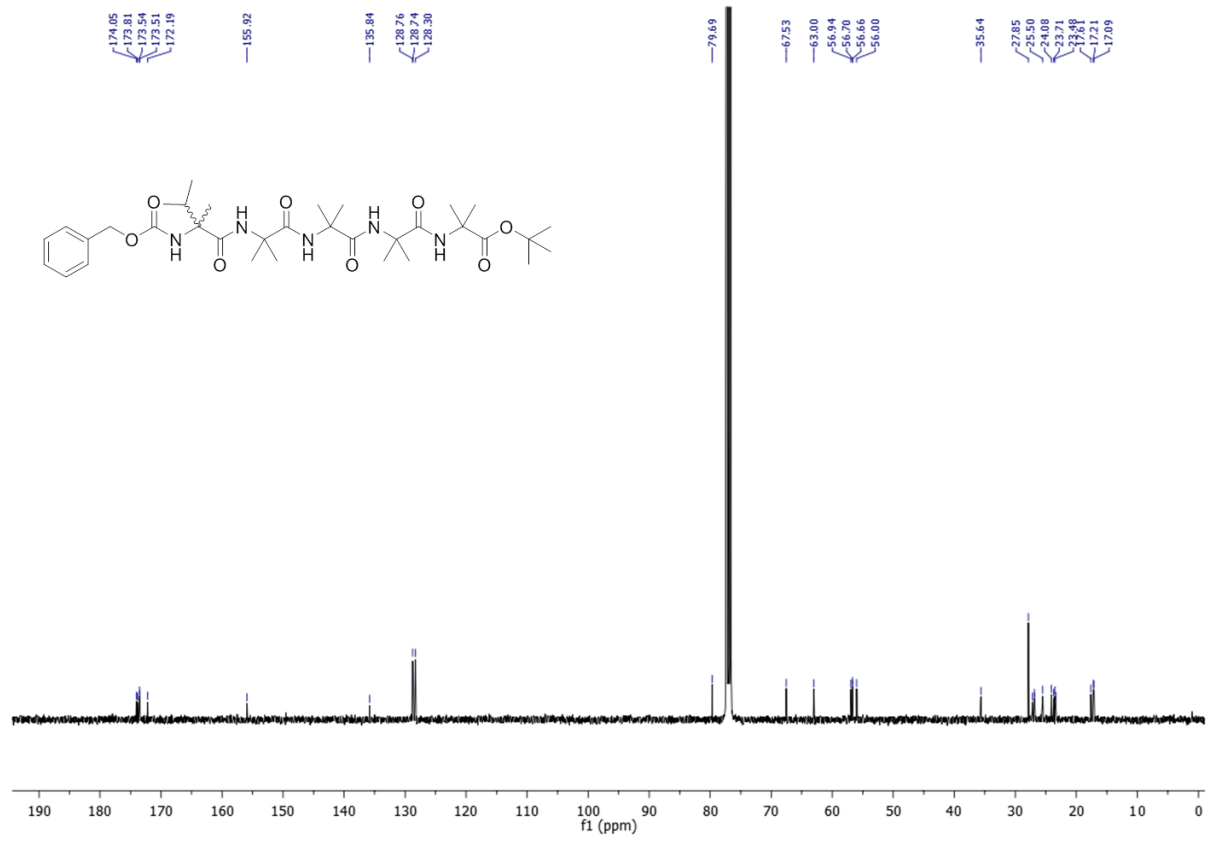

^{13}C NMR spectrum (75 MHz, $CDCl_3$) of Cbz-(*rac*)-(αMe)ValAib$_4$O^{t}Bu.

Analytical Experimental Section

Instrumentation: Fluorescence spectroscopy was carried out on a Perkin-Elmer LS55 fluorimeter. Temperature control was attained using a Julabo F25-HE water circulator. UV-visible spectroscopy was carried out using a Jasco V-600 spectrophotometer with the temperature controlled by a Jasco EHC-716 Peltier.

clogP values were calculated using the ClogP algorithms in ChemBioDraw Ultra 13.0, which are developed by BioByte (www.biobyte.com).

Preparation of stock peptide solutions: Stock solutions of compounds were prepared in methanol with final concentrations confirmed by UV-visible spectroscopy.

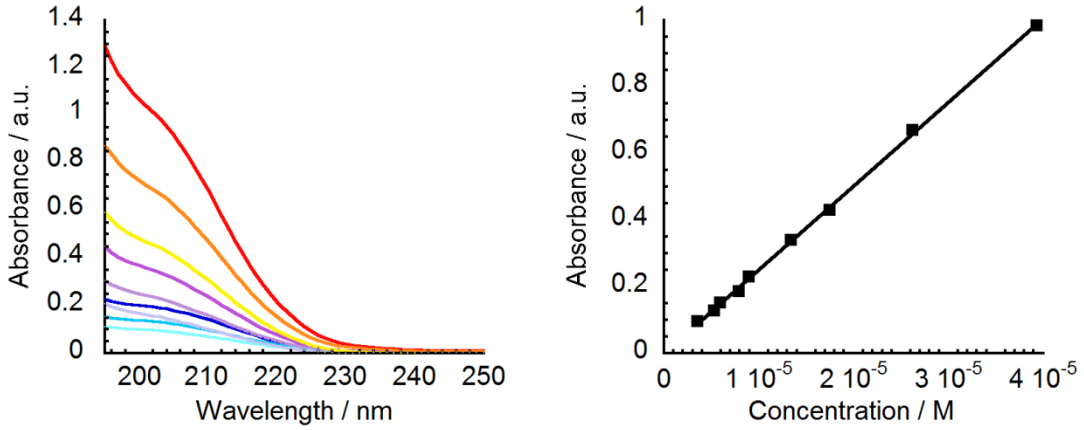

Figure S17: The changes in absorption spectrum of Cbz-L-Phe-Aib$_4$-O^{t}Bu in acetonitrile solution at 298K *(left)* together with the corresponding linear fit of the changes at 204 nm upon varying the transporter concentration *(right).*

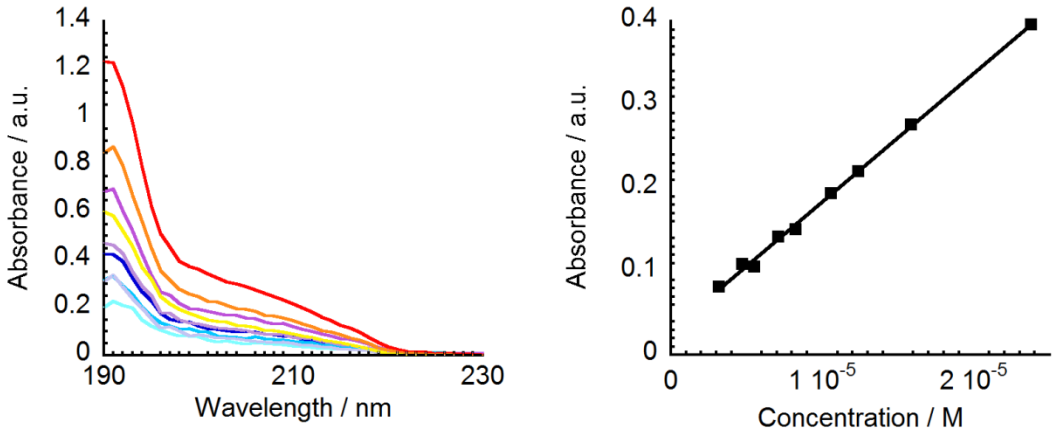

Figure S18: The changes in absorption spectrum of Cbz-L-MeVal-Aib$_4$-O^{t}Bu in acetonitrile solution at 298K *(left)* together with the corresponding linear fit of the changes at 198 nm upon varying the transporter concentration *(right).*

Preparation of 800nm large unilamellar vesicles

Egg yolk phosphatidylcholine (EYPC, 64 μmol) and cholesterol (16 μmol) were dissolved in spectroscopic grade chloroform. The solvent was removed *in vacuo* to give a thin film of lipid on the inside wall of the flask, which was dried further under vacuum for 1 hour. The thin film was rehydrated with 1.2 mL of trisodium 8-hydroxypyrene-1,3,6-trisulfonate (HPTS, 100 mM) dye in MOPS buffer (20 mM MOPS, 100 mM NaCl adjusted to pH 7.4 using NaOH). The thin film was detached from the sides of the flask by vortex mixing. The turbid suspension of lipids was then extruded 19 times through an 800 nm polycarbonate membrane in an Avestin Liposofast extruder to give a suspension of 800 nm large unilamellar vesicles. Excess (unencapsulated) dye was removed by gel permeation chromatography on PD-10 SEC columns (Sephadex G-25): 1 mL of the 800 nm vesicle suspension was diluted to 2.5 mL with stock MOPS buffer solution, loaded onto the GPC column, and the suspension run onto the column, before eluting the vesicles with 3.5 mL of MOPS buffer, giving a stock vesicle solution of 3.5 mL (final concentration of lipids = 15.23 mM). This solution of vesicles was used directly in the HPTS experiments.

Procedure for HPTS fluorescent assay of sodium ion transport

In a typical experiment, 100 μL of the resulting stock vesicle solution was diluted to 2 mL with stock MOPS buffer (final lipid concentration in cuvette 0.762 mM.). To this vesicle suspension was then added 20 μL of the principle compound in methanol and cuvette equipped with a stirrer bar. The cuvette was then placed in the fluorimeter with fast stirring mode assumed, and the fluorescence emission at 510 nm observed, resulting from the simultaneous excitation at 405 nm and 460 nm over a period of 45 minutes (2600 seconds). After three minutes (180 s) incubation at 25°C, 13 μL of a 1M $NaOH_{(aq)}$ solution was added, to provide the 'base pulse'. At 30 minutes (1800 s), 40 μL of a 10 % v/v solution of Triton X-100 detergent in MOPS was added to lyse the vesicles. Fluorescence time courses were normalised using the equation [S1]

$$I^n = (F_t - F_0) / (F_\infty - F_0) \qquad [S1]$$

where $F_0 = F_t$ at addition of base pulse, $F_\infty = F_t$ at saturation after complete leakage.

Procedure for the determination of first order rate constants

The normalised data (I^n) was iteratively fitted to first order kinetics using an equation of the general form:

$$I_{norm} = I_{\infty} - exp\ (kt + c) \qquad [S2]$$

The baseline (methanol only, no transporter compound) was then subtracted to give the final apparent rate constant value.

Sodium ion transport rates

For all sodium ion transport experiments, the HPTS assays were repeated several times and showed good reproducibility.

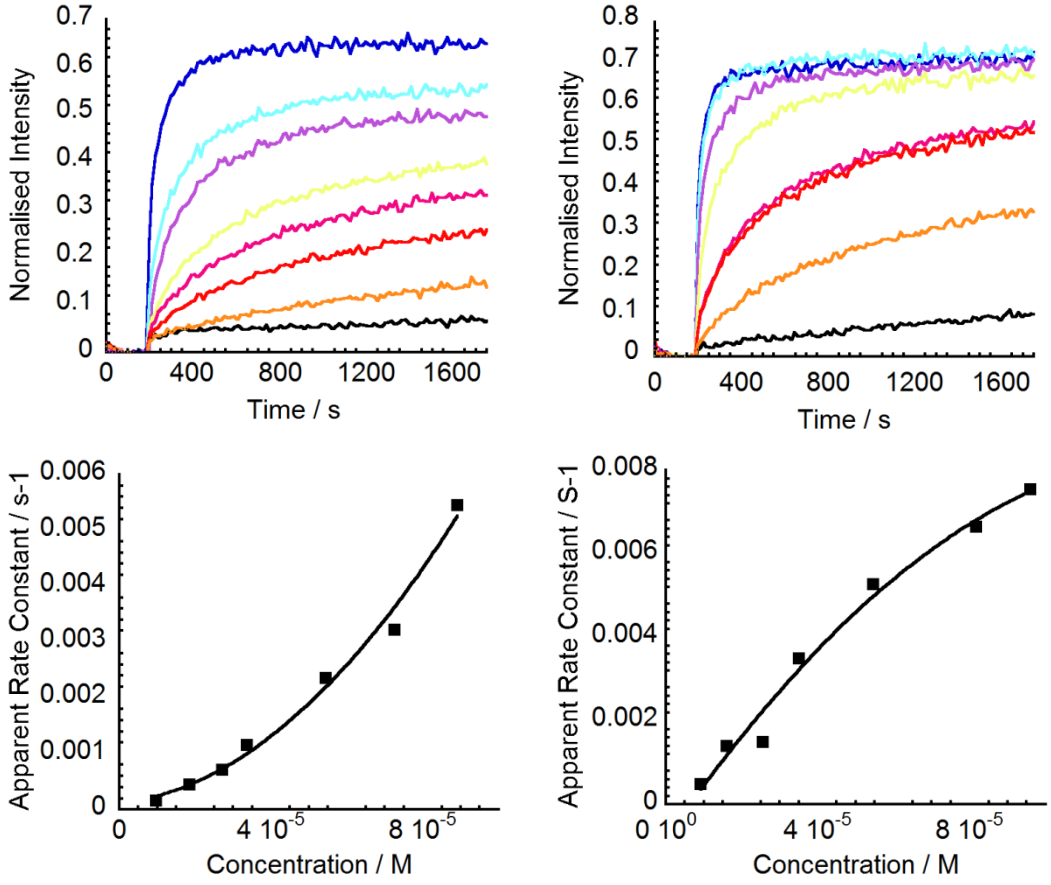

Figure S19: Enantiopure and racemic Cbz-Phe-Aib$_4$-O^{t}Bu HPTS profiles and rate data in 800nm EYPC vesicles with different transporter concentrations. Top: HPTS concentration studies, bottom apparent first order rate constants (methanol adjusted). *Left:* Cbz-L-Phe-Aib$_4$-O^{t}Bu *Right:* Cbz-Rac-Phe-Aib$_4$-O^{t}Bu. Stock transporter concentrations in methanol: Homochiral: 10mM, 8mM, 6mM, 4mM, 3mM, 2mM, 1mM, methanol in black. Racemic: 10mM, 8mM, 6mM, 4mM, 3mM, 2mM, 1mM, methanol in black. Final cuvette concentrations of transporter peptide are 100 fold more dilute than stock peptide solutions. Curve fits are to guide the eye.

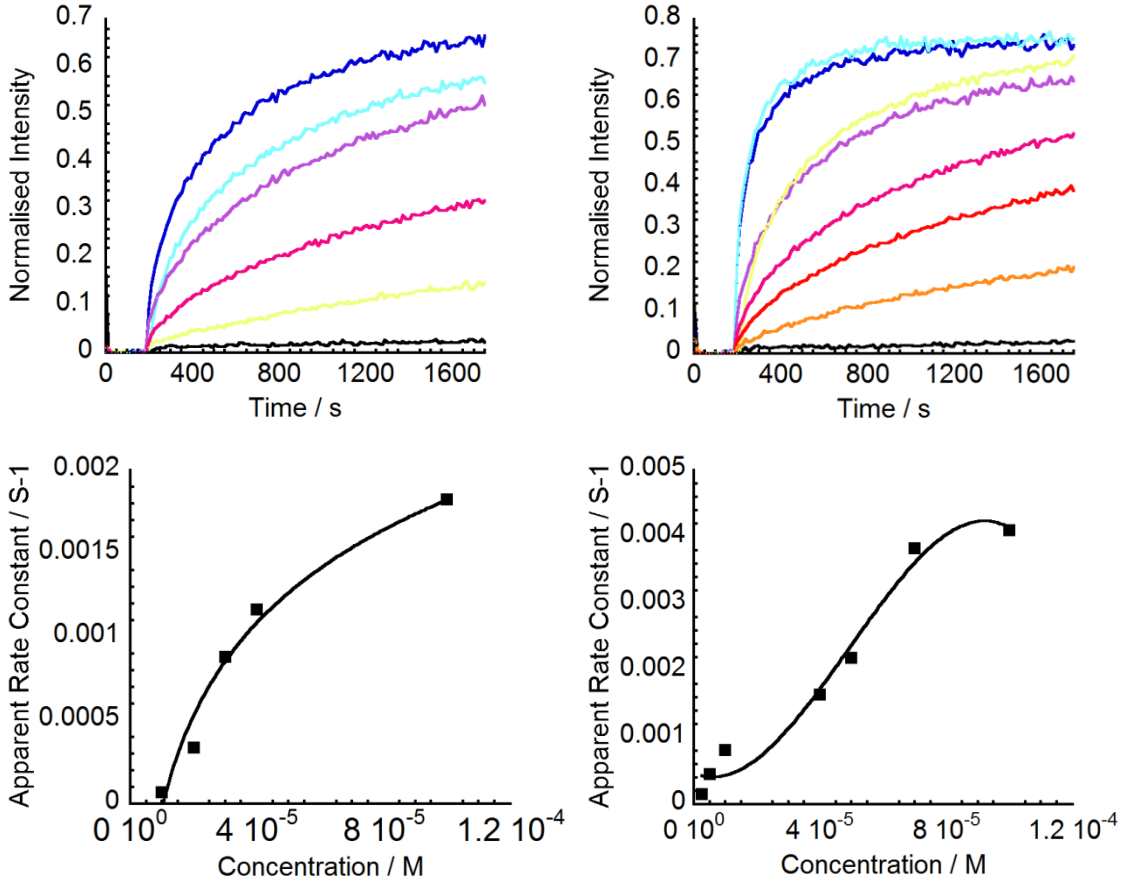

Figure S20: Enantiopure and racemic Cbz-MeVal-Aib$_4$-O^{t}Bu HPTS profiles and rate data in 800nm EYPC vesicles with different transporter concentrations. Top: HPTS concentration studies, bottom: apparent first order rate constants (methanol adjusted). *Left:* Cbz-L-MeVal-Aib$_4$-O^{t}Bu, *Right:* Cbz-Rac-MeVal-Aib$_4$-O^{t}Bu. Stock transporter concentrations in methanol: Homochiral: 10mM, 4mM, 3mM, 2mM, 1mM, methanol in black. Racemic: 10mM, 7mM, 5mM, 4mM, 1mM, 0.5mM, 0.25mM, methanol in black. Final cuvette concentrations of transporter peptide are 100 fold more dilute than stock peptide solutions. Curve fits are to guide the eye.

Fractional activity

Due to the increased propensity of the transporter peptides to self-aggregate, first order rate analysis of the transport experiments could not satisfactorily represent the kinetics of the system. Fractional activity allows the direct comparison of dye leakage caused by the synthetic transporters.[6,7]

Following normalisation of data, the baseline (methanol, no transporter) was subtracted from I^n to give I [S3]:

$$I = I^n - I^n_0 \qquad [S3]$$

The obtained I was further normalised into fractional HPTS emission I_F using equation [S4]

$$I_F = I / I_{MAX} \qquad [S4]$$

where I_{MAX} is a reference emission for the varied parameter of interest, in this instance, the maximum activity of the relevant transporter peptide in buffered solution before the addition of Triton X-100.

The term fractional activity Y is used to compare fractional HPTS emissions I_F at a given time, usually directly before the addition of Triton X-100 i.e. 1620 s after the start of the experiment.

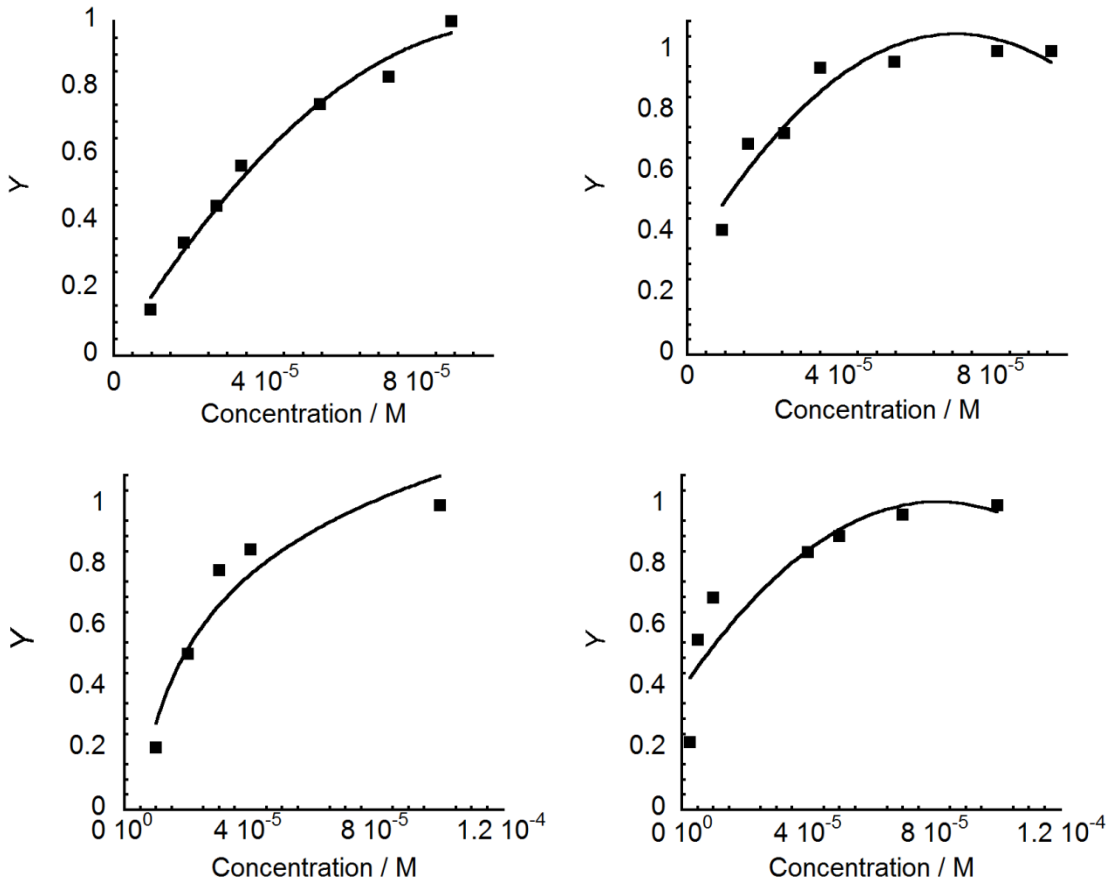

Figure S21: Fractional activity profiles in the HPTS assay in 800nm EYPC vesicles as a function of transporter concentration. *Top Left:* Homochiral Cbz-L-Phe-Aib$_4$O^{t}Bu, *Top Right:* Racemic Cbz-Rac-Phe-Aib$_4$O^{t}Bu. *Bottom Left:* Homochiral Cbz-MeVal-Aib$_4$-O^{t}Bu. *Bottom Right:* Racemic Cbz-Rac-MeVal-Aib$_4$-O^{t}Bu. Curve fits are to guide the eye.

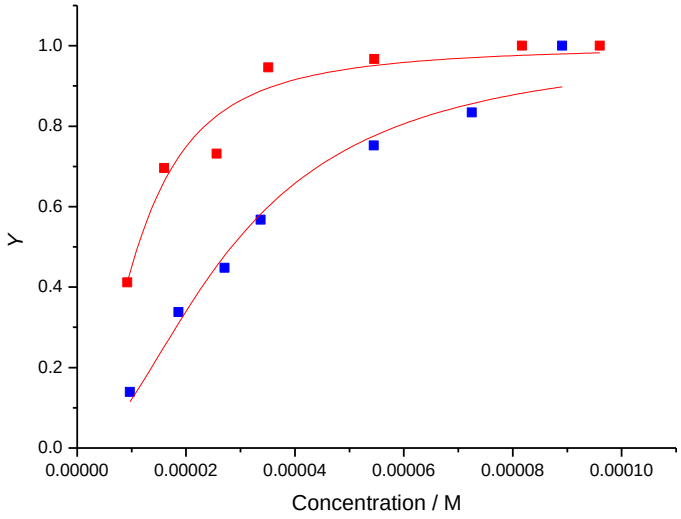

Figure S22: Comparison of fractional activity with increasing transporter peptide concentration, for racemic *(red)* and homochiral *(blue)* Cbz-Phe-Aib_4O^tBu.

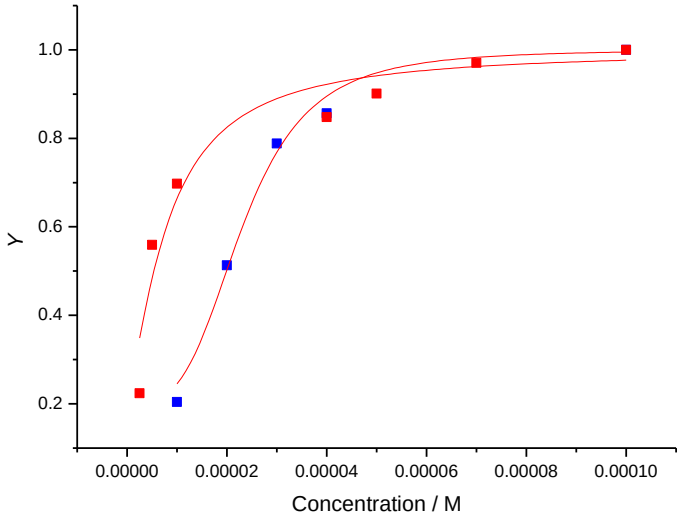

Figure S23: Comparison of fractional activity with increasing transporter peptide concentration, for racemic *(red)* and homochiral *(blue)* Cbz-MeVal-Aib_4-O^tBu.

5/6-Carboxyfluorescein release studies

The extent of release of 5/6-carboxyfluorescein from the phospholipid vesicles was measured by observing the 5/6-CF emission intensity at 517 nm following excitation at 492 nm.

EYPC-cholesterol (4:1) 800 nm vesicles were prepared as described above except with 1.2 mL of 5(6)-carboxyfluorescein (CF) (50mM) solution dissolved in MOPS buffer (20mM MOPS, 100mM NaCl, pH 7.4). In order to dissolve the 5/6-CF, sodium hydroxide (1M) was added dropwise until pH 11. The solution was then carefully acidified to pH 7.4 (1M, aq. HCl). Free 5/6-CF was removed by gel permeation chromatography on PD-10 SEC columns (Sephadex G-25) as per the procedure for LUV preparation. For each experiment, the initial (F_0) and total (F_{Triton}, 10% Triton X-100) fluorescence was determined and used to determine the final value: $(F-F_0)/(F_{Triton}-F_0)$.

Following normalisation of the 5/6-CF data, the background methanol was subtracted from the raw data, and the intensity of emission (I_F) plotted against concentration at a given time point, in this instance at 500 s after the start of the experiment, before the addition of Triton X-100.

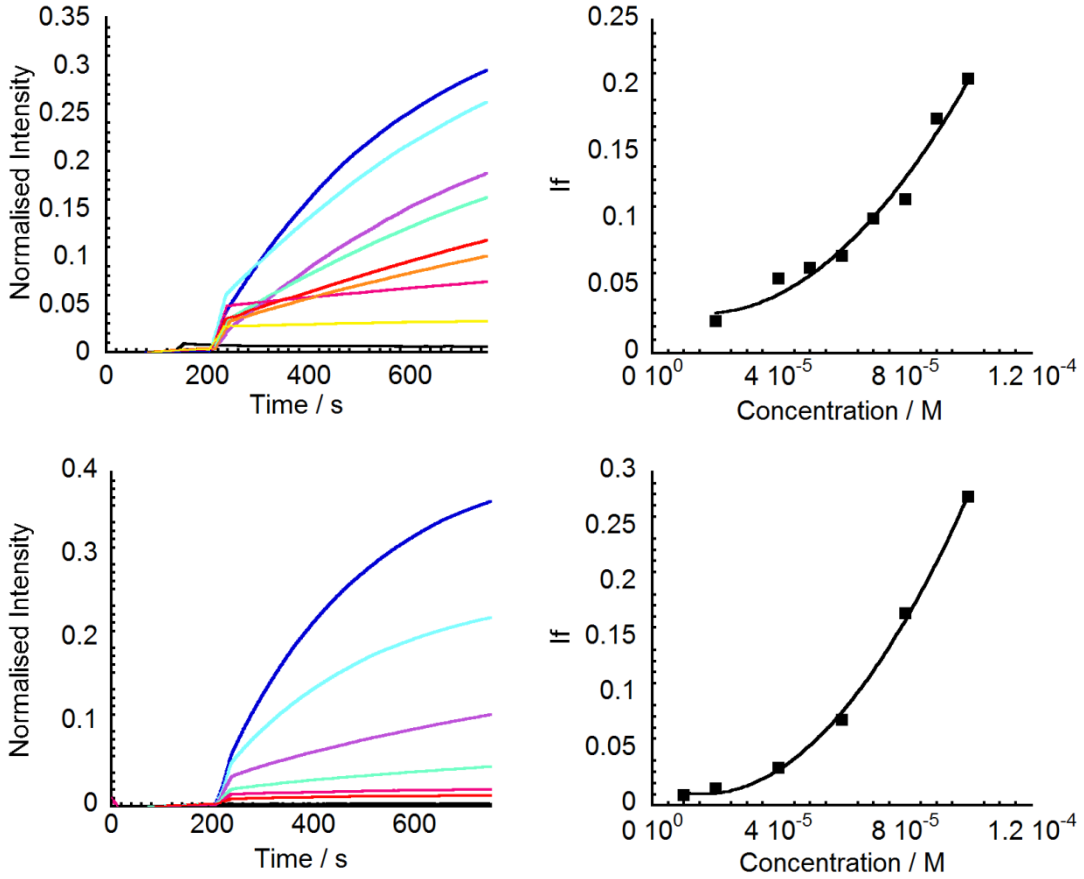

Figure S24: 5/6-Carboxyfluorescein release studies for Cbz-Phe-Aib$_4$-O^{t}Bu. Enantiopure and racemic Cbz-Phe-Aib$_4$-O^{t}Bu 5/6-CF concentration profiles *(left)* and fractional emission *(right)* data in 800nm EYPC vesicles with different transporter concentrations. Stock transporter concentrations in methanol: *Top Left*: Homochiral Cbz-LPhe-Aib$_4$-O^{t}Bu, 10mM, 9mM, 8mM, 7mM, 6mM, 5mM, 4mM, 2mM; *Bottom Left*: Racemic Cbz-Rac-Phe-Aib$_4$-O^{t}Bu 10mM, 8mM, 6mM, 4mM, 2mM, 1mM. Final cuvette concentrations of transporter peptide are 100 fold more dilute than stock peptide solutions. Fractional emission at 500 s is plotted against concentration for homochiral (*top*) and racemic (*bottom*) Cbz-Phe-Aib$_4$-O^{t}Bu. Curve fits are to guide the eye.

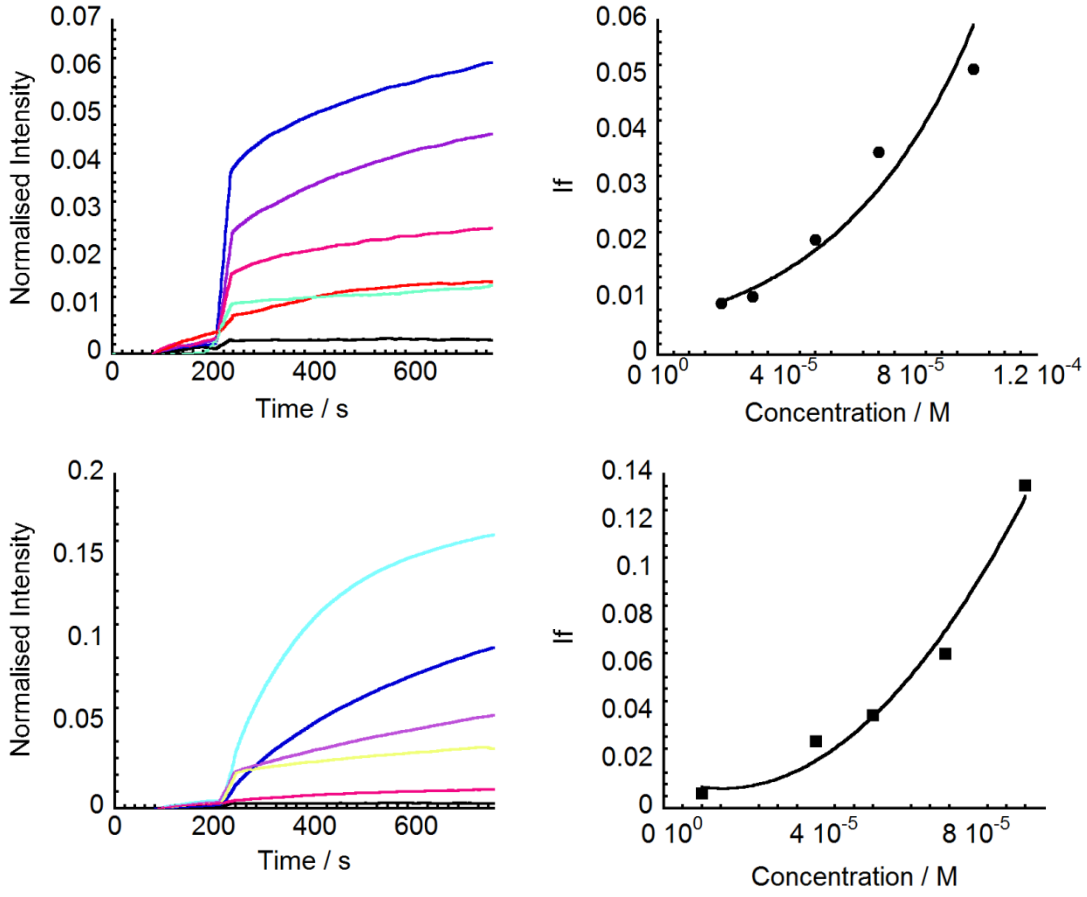

Figure S25: 5/6-Carboxyfluorescein release studies for Cbz-MeVal-Aib$_4$-O^{t}Bu. Enantiopure and racemic Cbz-MeVal-Aib$_4$-O^{t}Bu 5/6-CF concentration profiles *(left)* and fractional emission *(right)* data in 800nm EYPC vesicles with different transporter concentrations. Stock transporter concentrations in methanol: *Top left:* Homochiral Cbz-LMeVal-Aib$_4$-O^{t}Bu 10mM, 7mM, 5mM, 3mM, 2mM, methanol in black; *Bottom left*: Racemic Cbz-Rac-MeVal-Aib$_4$-O^{t}Bu 9.5mM, 7.5mM, 5.5mM, 4mM, 1mM, black in methanol. Final cuvette concentrations of transporter peptide are 100 fold more dilute than stock peptide solutions. *Right*: Fractional emission at 500 s is plotted against concentration for homochiral (*top*) and racemic (*bottom*) Cbz-MeVal-Aib$_4$-O^{t}Bu. Curve fits are to guide the eye.

Role of Lipid Chirality.

Although phospholipids have chiral headgroups the influence of that chirality on the organisation of components in the bilayers is either non-existent or very weak in the fluid phase (see references within M. Inagaki, M. Shibakami and S. L. Regen, *J. Am. Chem. Soc*., **1997**, 119, 7161-7162). More specifically with respect to ion channel function, it is known the function of the gramicidin ion channel does not depend on phospholipid chirality. An interesting example is described by Regen and co-workers,[10] who compared nearest neighbour recognition between racemates and enantiopure mixtures. They describe the differences observed as "modest", corresponding to only ΔG ~ 0.4-0.7 kJ/mol. For these reasons we do not believe lipid chirality would cause significant differences in the ionophoric activity of racemic vs enantiopure peptides within the accuracy limits of the HPTS assay, especially given the natural heterogeneity of these fluid phase EYPC lipid mixtures.

References

[1]. J. Clayden, A. Castellanos, J. Solà, G. A. Morris, *Angew. Chem. Int. Ed.*, **2009**, *48*, 5962.

[2]. L. Byrne, J. Solà, T. Boddaert, T. Marcelli, R. W. Adams, G. A. Morris, J. Clayden, *Angew. Chem. Int. Ed.*, **2014**, *53*, 151.

[3]. L. A. Carpino, A. El-Faham, *J. Am. Chem. Soc.*, **1995**, *117*, 5401.

[4]. (a) S. J. Pike, V. Diemer, J. Raftery, S. J. Webb and J. Clayden, *Chem. Eur. J.*, 2014, **20**, 15981–15990. (b) T. P. Pitner and D. W. Urry, *J. Am. Chem. Soc*., 1972, **94**, 1399-1400.

[5]. http://community.dur.ac.uk/j.m.sanderson/science/downloads.html

[6]. V. Gorteau, G. Bollot, J. Mareda, S. Matile, *Org. Biomol. Chem*. **2007**, *5*, 3000.

[7]. A. Vargas Jentzsch, D. Emery, J. Mareda, S. K. Nayak, P. Metrangolo, G. Resnati, N. Sakai, S. Matile, *Nature Commun*., **2012**, *3*, 905.

[8]. S. J. Pike, T. Boddaert, J. Raftery, S. J. Webb, J. Clayden, *New J. Chem*., **2015**, *39*, 3288-3294.

[9]. L. L. Providence, O. S. Andersen, D. V.; Greathouse, R. E. Koeppe II and R. Bittman, *Biochemistry*, **1995**, *34*, 16404-16411.

[10] M. Inagaki, M. Shibakami and S. L. Regen, *J. Am. Chem. Soc*., **1997**, *119*, 7161-7162